A Flow Cytometry Based Assay for the Quantification of Viruses Using Changes in Infected Cell Granularity

by

Megan Logan

A thesis
presented to the University of Waterloo
in fulfillment of the
thesis requirement for the degree of
Master of Applied Science
in
Chemical Engineering

Waterloo, Ontario, Canada, 2015

AUTHOR'S DECLARATION

I hereby declare that I am the sole author of this thesis. This is a true copy of the thesis, including any required final revisions, as accepted by my examiners.

I understand that my thesis may be made electronically available to the public.

Abstract

A need exists for rapid, low-cost, and accurate infectious viral quantification method in the bio-pharmaceutical field for the production of vaccines and virus-based therapeutics. Two of the most common and traditionally employed methods to quantify infectious viruses are plaque assays and cell culture infectious dose 50 ($CCID_{50}$); both are relatively inexpensive, however they can be time consuming and demonstrate significant variability, between experiments and operators. More recently developed methods use fluorescence to quantify viral components (e.g. DNA, protein, mRNA, etc), which allows for earlier enumeration, but cost and complexity are the major tradeoffs with respect to these techniques. Presented in this thesis is a novel method to quantify infectious viruses that is aimed at resolving the limitations of the aforementioned techniques; namely, marrying the traditionally mutually exclusive parameters of rapidness, economics, and variability. The proposed method seeks to quantify the infectious virions through the use of post-infection physiological changes within the cell using flow cytometry.

To validate this method, a complementary Vero cell line was infected with a replication-deficient herpes simplex virus type 2 mutant and monitored over a 72 hour period for changes in intracellular complexity, also known as granularity, using flow cytometry. Granularity can be measured using flow cytometry by recording the amount of light that bent at approximately 90° from the incident beam. This bending of light is most commonly caused

by light being reflected or refracted against internal cellular structures such as proteins or vesicles.

It was found that, between 16-20 hours post infection (hpi), the percentage of the infected cell population displaying an increased degree of granularity could be correlated with the viral titers obtained through a traditional plaque assay with R^2 values greater than 0.9 using a semi-logarithmic scale. To further demonstrate that this as a universal method, the technique was applied to Japanese quail muscles fibroblast cells (QT-35) infected with a highly attenuated canarypox virus (ALVAC). A similar increase in granularity corresponding to infection was detected in the infected population, thereby giving credence to the utility of this viral enumeration technique across a potentially broad virus-host cell range. Given the high level of correlation between the proposed and traditional methods of viral quantification, the use of flow cytometry could deliver cost savings and increase the throughput for use in the bio-pharmaceutical industry.

Acknowledgements

I would like to first and foremost express my gratitude to my supervisor, Professor Aucoin. Your continued patience, guidance, and criticisms over the past two years have been instrumental in my development as a researcher. I can't express how thankful I am that you were my supervisor.

I sincerely thank Professor Gorbet and Professor Moresoli for generously offering your time, feedback and guidance as readers of my thesis.

Many thanks to Arno Zeiser, Patrick Farrell and other members of the Sanofi Pasteur team, your willingness to help was always much appreciated.

I am especially appreciative to my lab mates in the Aucoin lab. It has been a pleasure working and seeing each of you every day. Jann and Sandi, I am so thankful to you for your support and advice through all of it. Your inputs have been invaluable, and I can't say how appreciative I am for having the opportunity to share the office with you two each day.

Lastly I would like to thank my dearest relationships. None of this would be possible without your support.

Dedication

I would like to dedicate this to my sister, Kirstyn Logan, for always being a role model for me, and giving me the tough love I needed.

Table of Contents

List of Figures

List of Tables

Nomenclature

ACAM529	Replication deficient herpes simplex 2 virus where the U_L5 and U_L29 are deleted from the viral genome
ALVAC	High attenuated canarypox virus
$CCID_{50}$	50% cell culture infectious dose assay
CNPV	Canarypox virus
CPE	Cytopathic effect
cDNA	Complementary DNA
dsDNA	Double stranded deoxyribonucleic acid
EEV	Extracellular enveloped virus
EGFP	Enhanced green fluorescent protein
ELISA	Enzyme-linked immunosorbent assay
FL1	Filter 1 (530/30)
FL3	Filter 3 (560 LP)
FSC	Forward scattered light
GFP	Green fluorescent protein
HEK293	Human embryonic kidney cells
HIV	Human immunodeficiency virus
hpi	Hours post infection
HSPG	Heparan sulfate proteoglycans
HSV	Herpes simplex virus
HSV-2	Herpes simplex virus type II
HVEM	Herpes virion entry mediator
ICP	Infected cell protein
IMV	Intracellular mature virus
INM	Inner nuclear membrane
LOD	Limit of detection
LOQ	Limit of quantification
MNA	Mouse neuroblastoma cells
MOI	Multiplicity of infection
mRNA	Messenger RNA
ONM	Outer nuclear membrane
PFU	Plaque forming unit
QT-35	Japanese quail muscle fibroblast cells
RT-qPCR	Real time quantitative polymerase chain reaction
RNA	Ribonucleic acid
rtPCR	Reverse transcriptase polymerase chain reaction
TGN	*trans*-Golgi Network
U_L	Unique long component of HSV DNA
U_S	Unique short component of HSV DNA

Vero	Green African monkey kidney epithelial cells
VHS	Virion host shut off protein

Chapter 1

Introduction

In recent years, increasing global demand has driven bio-pharmaceutical companies to endeavor to produce larger quantities of vaccines and other virus-based therapeutics while decreasing costs and improving efficiency of production and purification. Also, they must continue to adhere to strict government regulations to ensure the safety and efficacy of their products[1]. Some vaccines consist of live attenuated viruses or recombinant viral vectors to stimulate a patient's immune system to provide continuing immunity from a plethora of devastating diseases and infections, such as measles, mumps, rubella, smallpox, and hepatitis B and C[2]. The production and use of viruses is not limited to vaccines; viruses can be used as a delivery vehicle for therapeutics such as gene[3] and cancer[4,5] therapies and for production of therapeutics and other important biological molecules[6]. Currently, adeno-associated virus (AAV) has been approved for use in a gene therapy application (Glybera) by the European Medicines Agency (EMA) to treat lipoprotein lipase deficiency, and there are more than 1800 clinical trials ongoing for various gene therapies using viral vectors[3]. Similarly, viral vectors are important tools for production of biological molecules, such as the baculovirus expression vector system (BEVS) which has applications in human and animal vaccines[6]. With the ever increasing human population, the ability to produce large quantities of vaccines and therapeutics is of utmost importance to ensure the health of future generations.

In order to meet these needs, biopharmaceutical companies continue to search for improved methods to decrease cost and increase efficiency of production and purification.

Virus enumeration techniques are heavily relied upon to assess the efficiency of the production process, however they also often represent a significant bottleneck of production due to the time requirement to complete plaque assays or $CCID_{50}$ assays. Unlike small molecule drugs, which are often well-defined, chemically synthesized compounds having uniform molecular structure, viruses can be large, dynamic, multi-component bio-molecules with variable conformations and compositions, making them difficult to quantify[7]. To facilitate the optimization of virus production processes, it is necessary to have rapid, sensitive, and accurate methods to quantify and monitor the amount of viruses produced and retained during each step of the production process[8].

Currently, diagnostic testing for viruses can be divided into 3 main categories: assays for detection of 1) viral antigen; 2) viral DNA or RNA, and 3) infectious virus titer[9,10]. Viral antigen detection assays, such as the enzyme-linked immunosorbent assay (ELISA), detect the average level of viral antigen in a population using a highly specific antibody. Although very sensitive and specific, ELISAs yield qualitative data; the results cannot be accurately extrapolated to determine infectious titer due to the possibility of free-floating antigens in the sample solution. Viral genome measurement uses polymerase chain reaction (PCR) to amplify viral DNA or RNA in a sample of cells or the virus itself which offers advantages of speed and sensitivity, however the quantification of viral DNA cannot be used to determine an accurate infectious titer due to non-constant levels of viral DNA produced by cells. Antigen and DNA/RNA detection assays are ideal for quantifying DNA-based and subunit (protein) therapeutics and vaccines, but both suffer from their inherent lack of ability to

measure infectious viruses. Infectious titer is, therefore, the only method to accurately quantify infectious viruses because it quantifies successful infection events caused by mature virions. As stated, viruses are complex bio-molecules composed of protein components that undergo intricate and concerted assembly pathways to form mature virions that infect, replicate, and produce mature progeny viruses to extend infection. As such, measuring the amount of viral DNA/RNA or protein content in a sample quantifies only a fraction of the components that make up a virus, and gives limited information pertaining to infectious titer.

Previously, the methods employed to determine the infectious titer of viral particles have consisted of either the plaque assay or cell culture infectious dose ($CCID_{50}$) assay, which measures the number of plaques formed (i.e. cell lysis) or cytopathic effect of viral infection (i.e. abnormal cellular morphology), respectively. Both of these methods are labour-intensive, prone to operator bias and are time-consuming[11]. Furthermore, the methodology is crude, as the operator must manually count the number of infection "events" in multi-well plates, which offers significant opportunities for bias and error, leading to operator-to-operator variability.

Flow cytometry, on the other hand, has been identified as an appropriate tool for effectively estimating viral titer as an alternative to traditional methods[12–15]. It can be used to measure light scattering and emission of light using lasers to excite reporter molecules, such as fluorescent proteins, to provide qualitative and quantitative information about individual cells in a sample. Moreover, flow cytometry allows for rapid and sensitive measurement of

large numbers of “events”, allowing robust and powerful analysis of data of thousands of cells in a single sample.

Previous flow cytometric studies have used recombinant viruses that contain the green fluorescent protein (GFP) encoding gene[16,17], complementary cell lines that produce GFP upon infection[17,18], and immunostaining of viral glycoproteins to fluorescently label infected cells. These fluorescent cells can then be analyzed using flow cytometry to quantify the amount of the sample population that displays fluorescence which corresponds to infection[14,15]. Although these methods can be used to accurately estimate infectious viral titer, they involve additional staining steps or, in the case of viral-encoded GFP systems, are not favorable for use in vaccines. To circumvent the challenges associated with fluorescence detection, studies aimed at deducing and correlating the natural physiological effect of viral infection on host cells has shown great promise. Specifically, changes in granularity or intracellular complexity of cells has been observed during the course of infection with baculovirus and adenovirus[19–21].

1.1 Purpose of Work

The main goal of this work is to develop a method to quantify infectious viral particles using a high throughput method that requires less time than the plaque assay and $CCID_{50}$ while also reducing the potential for operator bias.

1.1.1 Hypothesis

We believe that a flow cytometric based method can be used to measure the granular changes in the cells post infection that can then be correlated to the initial infectious titer of the viral sample.

1.1.2 Objectives

The main goal of this work can be divided into smaller objectives:

1) demonstrate physical changes occur in the cells after exposure to the virus using flow cytometry;
2) identify the optimal parameters and time points to correlate granularity to initial viral infectious titer;
3) determine the accuracy and precision of the correlation and compare to the predicted titer obtained from traditional methods
4) determine if the assay can easily be transferred to another virus/cell system.

Described herein, we present a technique for quantification of infectious virus titer using flow cytometry.

Chapter 2

Literature Review

2.1 Herpes Simplex Virus

Herpes simplex virus type 2 (HSV-2) is among the most common sexually transmitted infections worldwide, and is the primary cause of genital and neonatal herpes, as well as genital ulcer disease[22]. An estimated 536 million people are infected worldwide. In the United States, an estimated 16% of adults test seropositive for HSV-2; however, only 10-20% of individuals diagnosed as infected with HSV-2 exhibit associated symptoms such as genital herpes[23]. There is also a growing body of evidence suggesting a link between HSV-2 and Human Immunodeficiency Virus Type 1 (HIV-1) infection, wherein the lytic-stage genital lesions caused by HSV-2 may serve as a portal for entry of HIV-1[24], with several epidemiological studies suggesting a 2- to 4- fold increase in risk of HIV-1 infection in HSV-2 positive individuals[25]. Clearly, there exists a need for an effective vaccination strategy to protect uninfected individuals from exposure to HSV-2 and recently there have been efforts made to produce a vaccine against HSV-2 which include subunit, live attenuated, DNA and single replication cycle vaccines[26–29].

2.1.1 Virus Structure

HSV-2 is an 150 nm enveloped virus encapsulating a single 155kbp linear double-stranded DNA (dsDNA) genome encoding approximately 74 genes[30,31]. The virus consists of a nucleus surrounded by an icosapentahedral capsid, a tegument layer and an envelope obtained from the host cell's membrane (Figure 1). The viral genome consists of two covalently linked segments, unique short (U_S) or unique long (U_L) sequences that are flanked by long inverted repeats and encode for at least 84 different polypeptides[32]. Many of the polypeptides have multiple functions, for example, the infected cell protein 27 (ICP27, encoded by U_L54) is an immediate early protein that is required for the transition from early to late viral gene expression, optimal DNA replication and inhibits pre-mRNA splicing[33]. The entire replication cycle of HSV takes approximately 22-24 hours.

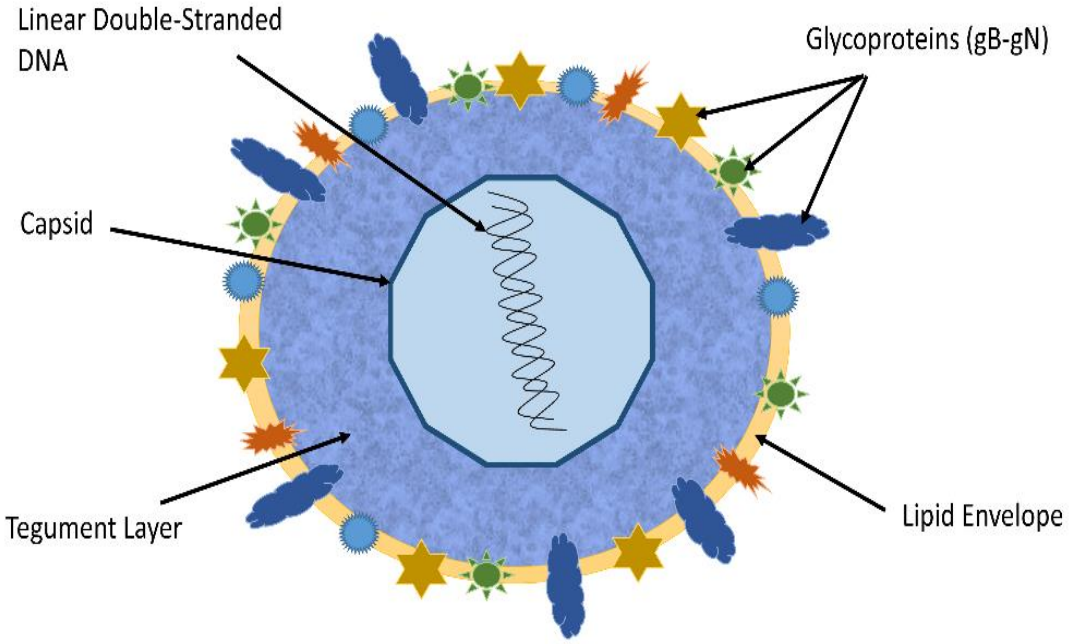

Figure 1- Structure of herpes simplex virus

The linear double-stranded DNA is encapsulated in an icosapentahedral capsid which is then surrounded by a layer of tegument proteins. The tegument layer is then surrounded by a lipid envelope which is taken from the host's plasma membrane and contains viral glycoprotein spikes that stick out and play numerous important functions.

2.1.1.1 Capsid

The 125 nm capsid of the herpes virus is made in the nucleus of the infected cell and consists of five conserved proteins: the major capsid protein, pUL19, which forms 162 capsomers (150 hexons and 12 pentons); two proteins, pUL18 and pUL38, which form the triplexes that interact and stabilize the capsomers; pUL35, which is found on top of all hexons; pUL6 which forms a portal for DNA packaging and release from the capsid[34–36].

2.1.1.2 Tegument

The capsid is coated with a tegument layer of at least 18 proteins that are obtained from the nucleus and cytoplasm of the cell. This layer is very complex and not completely understood at this point in time[37]. The tegument can be divided into inner and outer parts that are grouped together based on their association with the capsid[7,35,38]. Some of the most important tegument proteins include VP16, the virion host shutoff (VHS) protein, and VP 1-2[37]. VP16, also known as the α-trans-inducing factor (α-TIF), is an essential late-expressed protein that, upon infection is released into the cytoplasm with the other tegument proteins and induces early gene expression through the interaction with cellular proteins. It is also required for viral assembly and, in a complex with VP22, blocks mRNA degradation by U_L41[37]. VHS degrades cellular mRNAs as the virus enters the cell, suppressing expression of cellular proteins (including antiviral response) and allows the virus to maximize its own protein production[39].

VP 1-2 along with pUL37 binds directly to the surface of the capsid and possibly aids in the binding to microtubule motors during the transport of the capsid to the nucleus[38]. It has also been shown that the tegument proteins (pUL11, VP16, VHS, and VP22) aid in secondary envelopment by promoting the association of the capsid with the surface of the *trans*-Golgi network (TGN) that contains the viral glycoproteins[38].

2.1.1.3 Secondary Envelope

The outer envelope of the virus is a lipid bilayer acquired from the host and contains up to 10 glycoproteins (gB, gC, gD, gE, gG, gH, gI, gK, gL and gM) as well as at least two (U_L20 and U_S9) nonglycosylated intrinsic membrane proteins[37]. Glycoproteins J and N have not been found on the secondary envelope of the virus although there are two viral gene that code for them (U_s5 and U_L49.5 respectively) [37].

2.1.2 Infection Cycle

2.1.2.1 Viral Entry

In humans, genital mucosal epithelial cells are the target for primary infection and replication of HSV-2[40]. The virus attaches itself onto the cell by using three different types of cell-surface receptors (HVEM, nectin-1 and nectin-2) and then fuses its envelope to the cell's plasma membrane[32,41,42]. The initial binding is accomplished by glycoproteins C and B (gC and gB) which bind with heparan sulfate proteoglycans (HSPGs) that are on the cell surface[42,43]. It has been found that if gC and gB are deleted from the virus, binding to the cell

is greatly reduced and infectivity is eliminated. However, if only gC is absent, infectivity is greatly reduced, but not completely abolished, due to the reduced binding efficiency[44,45]. Although virus binding can happen anywhere on the surface of the cell, it has been recorded that the virus can attach onto F-actin rich membrane protrusions called filopodia via the gB-heparan sulfate interaction and connects the viruses to the retrograde actin flow which shuttles the virus to the cellular membrane (Figure 2)[46,47]. This process is called 'viral surfing' and the filopodia may provide an easy route for the virus to reach the cell body[43]. After the virion has been bound to the cell's surface it still must penetrate the cell, which it does by the fusion of the viral envelope to the plasma membrane (Figure 2)[43,48]. The virus can also enter the cell via endocytosis, which is when the cell takes up the virus into a vesicle. The virus can then escape the endosome by fusing with the endosome membrane after acidification[41,48].

There are four glycoproteins that are used to penetrate to the cell's surface: gB, gD, and the gH/gL heterodimer[43,49]. After the initial attachment, gD is required to bind with an entry receptor which causes a conformational change in gD which then triggers conformational changes in gH/gL and gB that lead to the fusion of the viral envelope to the cell membrane[42].

Once the membranes of the host cell and virus have fused, there is a release of the tegument proteins along with the capsid into the cytoplasm. One of the major roles of the inner tegument proteins is to recruit and bind to microtubule motors to transport the capsid to a nuclear pore in order to release HSV's DNA into the nucleus[37]. When the capsid has reached a nuclear pore VP1-2 and nucleoporins Nu358 and Nup214 create a complex such that the

portal on the capsid (pUL6) sits on top of the nuclear pore and the DNA is subsequently released into the nucleus where gene expression and viral replication can begin [49].

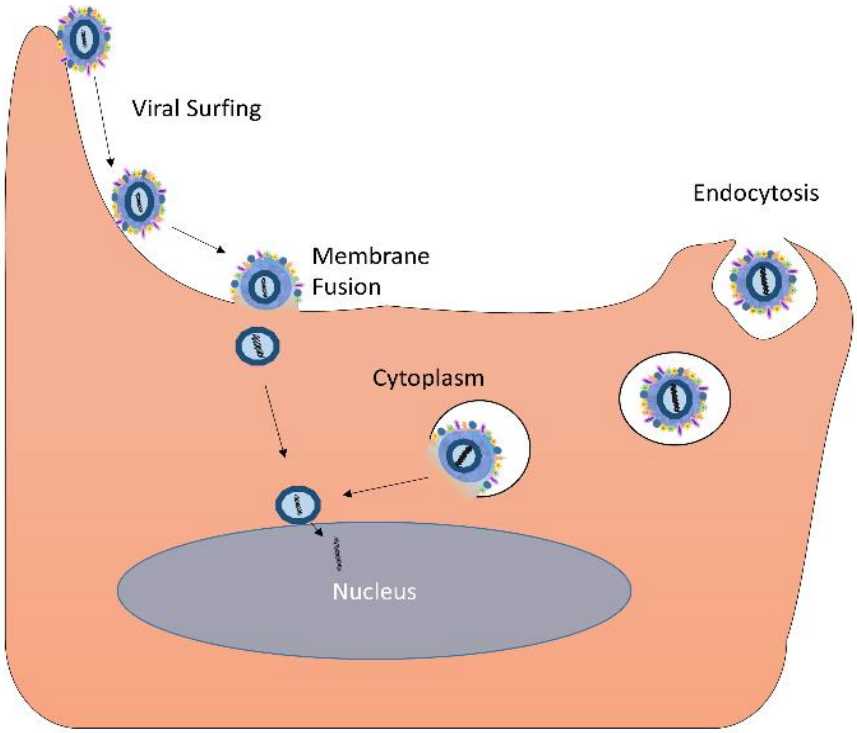

Figure 2- Herpes simplex virus entry into the cell

The virus can attach onto the cell's filopodia which are arm-like extensions of the cell which contain F-actin rich regions that the virus can initially bind onto and then 'surf' towards the main body of the cell where the virus will fuse membranes with the cell's plasma membrane through interactions between gB, gD, gH/gL and HSPGs on the cell's surface. The alternate mechanism of infection is the virus being engulfed by the cell and transported into the cell through an endosome where then virus then fuses membranes with the endosome[41]. Both methods of entry result in the tegument proteins being released into the cytoplasm and the capsid being transported to the nucleus where the viral DNA is discharged.

2.1.2.2 Viral Gene Expression

After the viral DNA has entered the nucleus of the cell it circularizes and the virus begins harnessing the cellular machinery (specifically host RNA polymerase II) to begin translating viral DNA at localized replication sites[37]. HSV has three main phases of gene expressions, immediate early (α), early (β), and late phase (γ) which regulate each other in a cascade fashion[37]. The α genes are the first to be transcribed with the aid of the tegument protein VP16 which is a γ protein. The expression of α genes is autoregulated by the accumulation of α proteins such as the infected cell protein 4 (ICP4) and ICP0. These two products of the immediate early phase also serve to up-regulate the expression of β and γ_1 (leaky-late) genes. β proteins are enzymes and DNA-binding proteins that are involved in viral DNA replication which then lead to the activation of γ genes[37]. The γ genes code for the glycoproteins and are involved with the assembly of the final virus progeny.

2.1.2.3 Replication

The transcription of the viral DNA, replication of DNA and capsid assembly all occur inside localized replication sites within the nucleus of the cell. The first step of HSV-2 replication is the duplication of its DNA, which is believed to be conducted through a two-stage process where it is initiated by binding to U_L9 and then the formation of a replication complex[37]. The viral proteins that are involved include a viral DNA polymerase catalytic subunit and its processivity factors (U_L30, U_L42), the origin binding protein (U_L9), a single stranded DNA binding protein (U_L29), and the helicase-primase complex (U_L5, U_L8, U_L52)[37]. It is also

presumed that host cell factors are also involved in the replication, which could include such proteins as DNA polymerase α-primase, DNA ligase, and topoisomerase II[37]. The DNA replication process begins as U_L9 and U_L29 (also known as infected cell protein 8 (ICP8)) bind to the viral DNA inside the nucleus of the cell at specific origin binding sites (OriL and OriS), separating the two strands of DNA[50]. Then the viral helicase-primase complex and polymerase bind at the replication forks and it is thought to begin replication through theta replication, but then switches to rolling circle replication through an unknown mechanism (Figure 3). The rolling circle mechanism produces long concatamers which are later cleaved before being packaged into the capsid[37]. More recent studies have hypothesized that HSV DNA replication is very complex and involves recombination-dependent replication like that of lambda phage[50–52].

One of the methods for creating a vaccine against HSV-2 is to create mutants that are unable to replicate their DNA. The HSV-2 mutant called ACAM529 has both the U_L5 and U_L29 (ICP8) deleted from the virus' genome. Therefore the virus cannot replicate its DNA in a non-complementary cell line. It is important to note that ICP8 does not solely act as a single stranded DNA binding proteins, but also stimulates several other viral DNA replication proteins such as U_L9 and the helicase/primase complex[37]. ICP8 is also required for localization of viral and cellular proteins in nuclear compartments or 'prereplicative sites' within the nucleus as well as possibly playing a scaffold role for HSV DNA replication complexes[37].

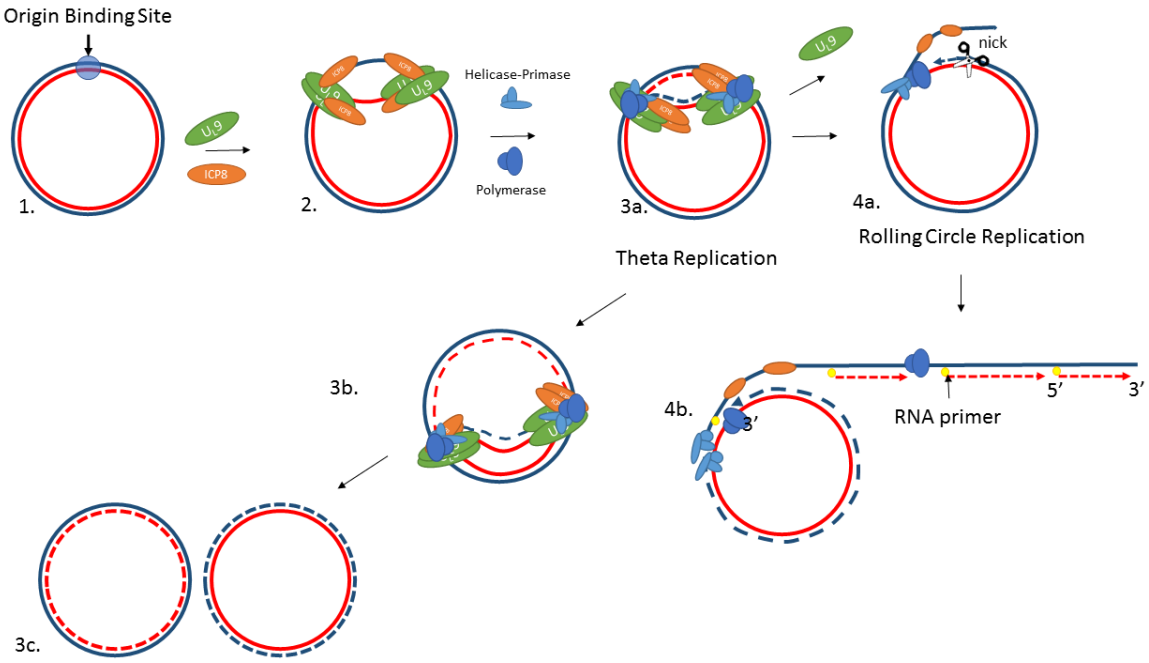

Figure 3- Model of herpes simplex virus DNA replication

1. After being released into the nucleus, the viral DNA quickly circularizes and then 2. U_L9 (the origin binding protein) binds to one of three specific viral origins of replications sites (one OriL or two OriS) and begins to unwind the DNA and recruits ICP8 (the single-stranded DNA binding protein) onto single stands of unwound DNA to prevent the DNA from reannealing[50]. 3a-c. The remaining 5 proteins are then recruited (U_L5, U_L8, U_L52, U_L30, U_L42) to form a helicase/primase complex at the replication forks and theta replications is used to replicate the viral DNA. 4a. The replication changes from theta replication to a rolling circle mechanism through an unknown mechanism by removing U_L9 and making a nick[37]. The helicase/primase complex will unwind the DNA and begin replicating the DNA from the 3' → 5' end while ICP8 binds to the single stranded DNA that is displaced by the leading strand. 4b. As the replication continues the displaced strand rolling circle replication will produce concatamers of viral DNA which will be cleaved before they enter the capsid.

2.1.2.4 Viral Assembly and Egress

After the production of the capsid components (γ proteins), viral DNA and glycoproteins, the capsid components autocatalytically begin to form the capsid in the nucleus which involves the hexons, pentons, triplex proteins, pUL26 and an additional pUL26.5 scaffold protein[35]. The DNA is then packaged into the capsid by cleaving the concatamers before they enter the capsid. It has been shown that 3 different types of capsids form; capsids without DNA or scaffold proteins (type A), capsids that only have the scaffold proteins (type B), and capsids that have both the DNA and scaffold proteins (type C)[37].

There are three proposed mechanisms of how the mature capsid exits the nucleus; 1) an envelopment-deenvelopment model, 2) nuclear pore model and 3) a single envelopment model[37,38,53,54] (Figure 4). The envelopment-deenvelopment pathway was first suggested by Stackpole in 1969 and hypothesizes that the capsid buds through the inner nuclear membrane into the perinuclear space and then fuses membranes with the outer nuclear membrane to release the capsid and tegument proteins into the cytoplasm[55]. The nuclear pore model has recently been proposed by Wild *et al.* in which capsids could exit the nucleus by passing through enlarged nuclear pores. Through electron microscopy, they demonstrated that during early infection the number of nuclear pores decreases and enlarged nuclear pores (140 nm in diameter) form in which capsids could exit through[53,56]. The single envelopment pathway is credited to Johnson and Spear in 1982 and theorizes that the capsid buds through both the inner and outer nuclear membrane into the cytoplasm[57].

Although there is evidence to support and oppose each pathway, there is greater support for the envelopment-deenvelopment pathway in the scientific community due to a growing body of evidence in favour of it[38,54]. The consequences of these different pathways are the number of membranes the capsid contains after it exits the nucleus as well as where the tegument layer is formed. For example, in the envelopment-deenvelopment pathway the tegument layer is initially added in the nucleus, then further modified in the cytoplasm, and then the glycoproteins and outer membrane is added by the Golgi apparatus before the virus exits the cell. In contrast, the single envelopment pathway states that the tegument layer is solely added in the nucleus, and the outer membranes and glycoproteins are obtained from the inner nuclear membrane and then the immature glycoproteins are further processed through interactions with the Golgi apparatus[57,58].

An interesting aspect of HSV is its ability to spread via cell-to-cell. Studies have shown that in polarized epithelial cells, the herpes virus has the ability to direct its budding to the basolateral surface of the cell and more specifically to cell-cell tight junctions[37,38]. Glycoproteins gE and gI are believed to accumulate in parts of the TGN that are destined for the basolateral surface of the cell and promote secondary envelopment at these sites[59–61]. One benefit of cell-to-cell spread is evasion of the innate and adaptive immune defenses such as antibodies and phagocytes that target viruses in extracellular space[62].

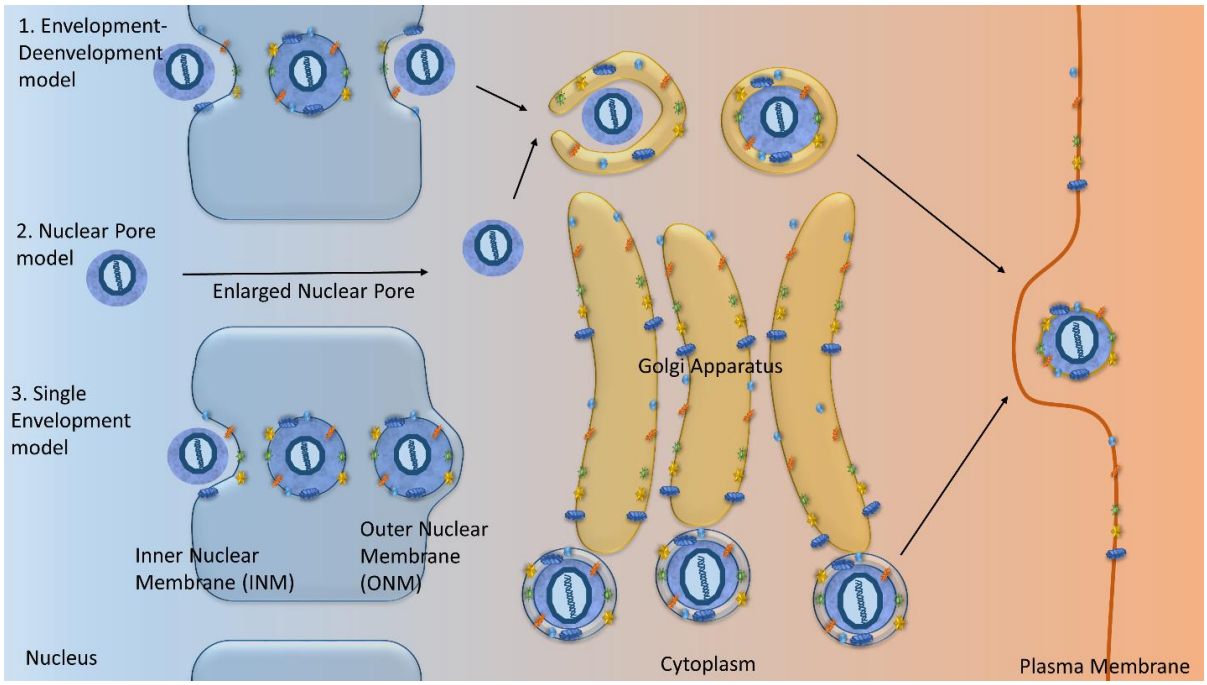

Figure 4- Proposed mechanisms of viral egress

There are three proposed modes of viral egress through the cell. 1. The envelopment-deenvelopment model states that the capsid along with some of the tegument proteins are enveloped by the inner nuclear membrane (INM) and then become deenveloped by the outer nuclear membrane (ONM). The capsid with the tegument proteins are then released into the cytoplasm, where more tegument proteins are added in the cytoplasm and the capsid becomes enveloped by cytoplasmic vesicles. The vesicles are then released from the *tans*-Golgi network (TGN). The virus then fuses membranes with the plasma membrane and is released outside of the cell. 2. The nuclear pore model proposes that the capsid exits the nucleus through enlarged pores to approximately 140 nm and then follows the same path as the envelopment-deenvelopment pathway[53,56] 3. The last mechanism proposes that the capsid will obtain two membranes by budding through both the INM and ONM and as it travels through the cytomplasm it joins with the Golgi, where the glycoproteins can be modified. The membrane obtained from the ONM will then fuse with the plasma membrane and release the virion outside the cell.

2.2 Canarypox Virus Vectors

Canarypox virus (CNPV) is an avipoxvirus that has the ability to infect and strongly express heterologous antigens in mammalian cells, but it is unable to complete its replication cycle in primate cells which has made it a very attractive vaccine candidate (Table 1)[63,64]. In addition to being unable to complete its replication cycle in non-permissive cell types, prior exposure to other orthopoxviruses does not neutralize CNPV and therefore does not reduce the immunogenicity of the virus. Furthermore, CNPV does not elicit high levels of neutralizing antibodies, and consequently this viral vector can be used multiple times without reduced efficacy[65]. ALVAC, a plaque isolate of the canary vaccine Kanapox, has previously been developed for veterinary medicine to treat avian and equine influenza[65]. Although currently there is no commercially available vaccine using CNPV available for humans, vaccines against HIV, metastatic colorectal cancer and malaria are being developed and are in various phases of clinical trials (Table 1)[63,65–70].

Table 1-ALVAC vector based vaccines

Target Pathogen	Target Species	Insert	Commercial Use	Reference
Rabies virus	Cats	Glycoprotein G	Yes	71
Canine distemper virus	Dogs, ferrets	Fusion protein, hemagglutinin	Yes	72
West-Nile virus	Horses	Pre-membrane and envelope proteins	Yes	73,74
Feline leukemia virus	Cats	Envelope glycoprotein	Yes	75,76
Equine influenza	Horses	Hemagglutinin	Yes	77
Hepatitis B	Chimpanzee	Surface antigen	No	78
HIV-1	Humans	gp160 and gp120, LIPO-5	No	68,69
Malaria	Humans	Circumsporozoite protein	No	66
Melanoma	Humans	gp100, Mage 1, Mage 3	No	4
Hepatitis C	Humans	Structural and non-structural proteins	No	79
Colorectal Cancer	Humans	Carcinoembryonic antigen, p53	No	4,67

2.2.1 Virus Structure

CNPV is a large enveloped brick-shaped virus that has dimensions of 270 x 350 nm and contains a single linear double-stranded DNA that contains 365 kbp, surrounded by a core membrane, lateral bodies (function unknown) and a surface membrane (Figure 5)[80,81]. The genome contains approximately 328 possible genes[81]. It has two distinct infectious forms: extracellular enveloped virus (EEV) and intracellular mature virus (IMV). These two forms differ by their lipid membranes and surface proteins that have yet to be fully characterized[65]. The IMV is the most abundant form of infectious virus produced from the host cell. There is limited research on CNVP which has resulted in very little information available about this particular virus.

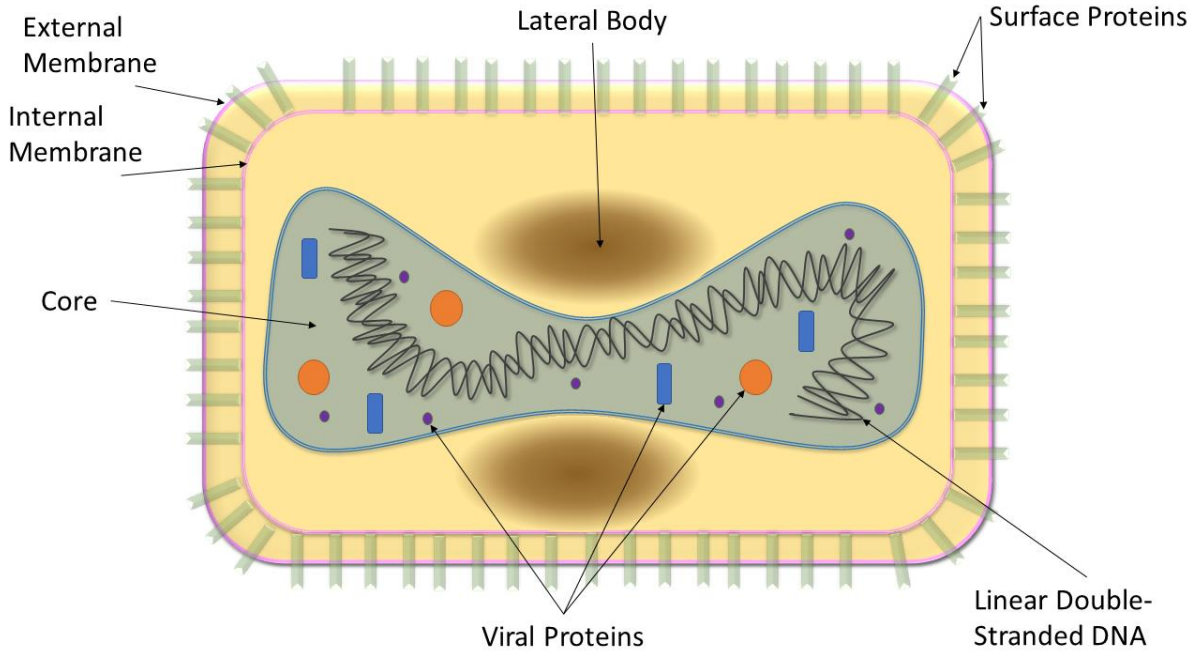

Figure 5- Canarypoxvirion structure

CNVP is a large virus (270 x 350 nm) with a relatively large genome (365 kbp). The linear double-stranded DNA and viral proteins such as transcription factors and RNA polymerases are encapsulated in the core which has a dumbbell shape with two lateral bodies on either side[65]. The difference between IMV and EEV is the lipid membrane and the surface proteins. The IMV can be released through cell lysis and therefore only has the internal membrane, while the EEV gains a second double membrane from the TGN and buds through the host cell's plasma membrane to exit the cell[82].

2.2.2 Infection Cycle

To begin infection, the virus binds to the cell membrane and then must enter the cell, which is accomplished through direct membrane fusion to the outside of the cell, or endocytosis[64]. Unlike HSV, CNPV replicates in the cytoplasm of the host cell. Upon entry, the viral core, which contains the viral RNA polymerase and transcription factors, begins to synthesize viral mRNA as early gene expression begins[65]. The core then degrades, and the viral DNA is free in the cytoplasm and the intermediate viral gene transcription occurs triggering genomic DNA replication[65,82]. Late gene expression produces all the structural protein, and the progeny virions begin to assemble in 'virus factories' which are inclusion bodies formed in the host cell[65,82]. It is believed that the inclusion bodies are the sites of active viral replication and assembly at these sites act to concentrate proteins, nucleic acids and other molecules essential for virus production[65,83]. From the viral factories, circular immature viral particles are produced and mature through a series of unknown maturation steps. The mature virions exit the cell through three different methods: cytolysis, virus-induced exocytosis or by budding[65]. Cytolysis occurs when the cell lyses after sustained cytopathic effect (CPE) and IMVs are released into the supernatant. Virus-induced exocytosis does not destroy the cell, but rather the IMVs are packaged into vesicles and are transported to the plasma membrane and are released into the extracellular space[65]. Viral budding is the only method that produces EEV, since the virus obtains a secondary double membrane from the TGN and then the outer side of the membrane can fuse with the plasma membrane, releasing the virion into the extracellular space[65]. One complete viral replication cycle takes approximately 3-4 days[64].

2.3 Virus Enumeration Techniques

There exists a multitude of methods for the quantification of viruses. During the amplification of viruses and viral vectors for commercial or large scale production, it is important to quantify virus yield after each step to assess the efficiency of the process. The quantification of the virus is often a slow process due to the complex nature of viral particles. Currently, rapid quantification methods for viruses include viral antigen detection assays, viral DNA assays, and flow cytometry based methods[84]. The oldest and most commonly used assays to determine the infectious titer are infectious virus titer assays such as the plaque assay and cell culture infectious dose ($CCID_{50}$) assay, which are both labour-intensive and time-consuming[11]. Methods for the quantification of HSV and ALVAC are discussed along with a general overview of other commonly used viral quantification methods.

2.3.1 Quantification Methods for HSV

2.3.1.1 Plaque Assay

The plaque assay is one of the oldest and most commonly used methods to titer virus and it relies on the virus' ability to cause cell lysis which is visually observed as clear plaques in a confluent monolayer of cells. To perform this assay a healthy, a confluent layer of cells is infected with a serially diluted solution of virus. After the virus has attached to the cell, a viscous overlay media is added to ensure that the infection can only spread to adjacent cells. The viral stock must be sufficiently diluted such that it results in 50-200 plaques formed per well so the observer can accurately score the plate (Figure 6). If the concentration of virus is

too high, then the plaques will be indistinguishable from each other and a proper count cannot be recorded, as can be seen in Figure 6.

Once the plate has been scored the initial viral titer can be estimated by the following equation:

$$Viral\ Titer = \frac{D \times P}{V} \qquad \text{Equation 1}$$

where:
D is the dilution of virus
P is the average number of plaques counted
V is the volume of diluted virus sample added to the monolayer of cells

This is a powerful method because it directly quantifies the number of infectious viral units since one plaque forming unit (PFU) correlates to a single virion that has lysed and spread to adjacent cells in the culture, creating a single plaque. However, this assay is prone to operator bias due to the dependence on the operator's ability to distinguish single plaques, which are not always perfectly circular or unattached. Another major problem with this assay is that in order for visible plaque to form, an incubation time of 2-9 days (depending on the life cycle of the virus) is required before accurate results can be obtained[13]. For continuous processing or optimization of the manufacturing process, these time delays can seriously hinder the progress of the process development.

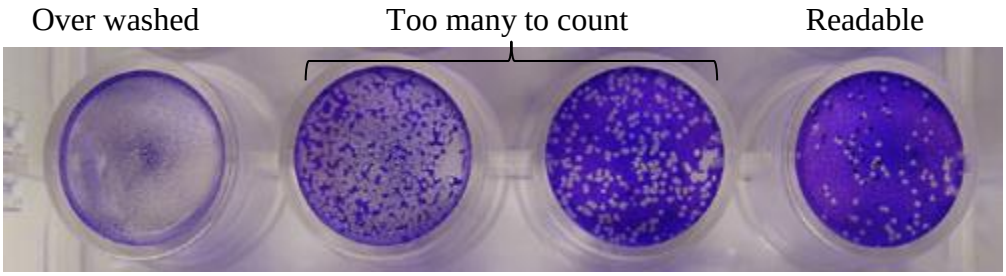

Figure 6- Sample plaque assay

A plaque assay was performed with a serially diluted virus sample. Each plaque represents one infectious virion, but if the sample is too concentrated there will be too many plaque to count, or individual plaques will be difficult to identify. Also some plaques are irregularly shaped or can be along the edge of the well which makes them difficult to identify. It is up to the technician to properly prepare the plate such that the cells do not get washed away, and there are approximately 50-200 plaques per well. The technician also must be able to accurately distinguish and count individual plaques which will affect the calculated initial concentration of the virus stock.

2.3.1.2 Real Time Quantitative Polymerase Chain Reaction (RT-qPCR)

Real Time Quantitative Polymerase Chain Reaction (RT-qPCR) has been used to estimate the infectious viral titer of HSV based on the viral RNA content of cells that have been infected with serially diluted virus[9,85,86]. This method involves seeding a 96-well plate with cells and then infecting the monolayer of cells with serially diluted virus, along with assay standards and controls, after a certain length of time, the viral RNA is extracted from the cells. A reverse transcription reaction is done to convert the RNA into complementary DNA (cDNA) using a reverse transcriptase and then this cDNA is amplified using specific primers, deoxyribonucleotides and a thermo stable DNA polymerase along with a fluorophore that will fluoresce upon binding to dsDNA (for example SYBR Green or TaqMan®). The cDNA will be amplified using a thermal cycler and the relative fluorescence will be monitored. Using a standard set of viral dilutions, the fluorescence obtained at a specific cycle number can be correlated to the viral concentration of the sample.

Aziz *et al.* developed an infectious titer assay using RT-qPCR for ACAM529 by seeding a 96-well plate and infecting with 50 μL of viral dilution and then collecting the RNA after 16 hpi and performing one-step RT-qPCR. They found that there was a linear relationship between the logarithm of viral titer and cycle number using the gD2 gene for time points 12-16 hpi.

This method is preferred for sensitive and quick analysis and it also has the added benefit of detecting virus in clinical samples, since primers are designed to target select genes that can

be unique to a particular virus. The disadvantages of this method is that it has a higher cost and complexity than the plaque and $CCID_{50}$ assays since it requires specialized equipment, costly reagents and numerous processing steps[9].

2.3.2 Quantification Method for Canrypoxvirus

2.3.2.1 Endpoint Dilution Assay

The 50% Cell Culture Infectious Dose ($CCID_{50}$) is a method developed by Reed and Münch, that calculates the titer where 50% of a cell culture demonstrates CPE[87]. Monolayers of cells are cultured on 96-well plates and infected with serially diluted virus and incubated until CPE can be observed (5-8 days)[13]. The plates are then scored based on the number of wells per dilution that display CPE and the 50% infectious dose is calculated by the following equation [87,88]:

$$M = 10^{\left[x_1 - \left(\left(\frac{y_1 - 50}{y_1 - y_2}\right) \times logh\right)\right]} \qquad \text{Equation 2}$$

where:
y_1 is the viral dilution in which the percent of wells that display CPE is ≥50%
y_2 is the viral dilution in which the percent of wells that display CPE is ≤50%
x_1 is the log of the dilution of the viral dilution of y_1
h is the log of the dilution factor
M is the $CCID_{50}$ titer

The $CCID_{50}$ titer is the amount of virus required for 50% of the wells to become infected, given a certain volume, dilution and incubation time. To translate the $CCID_{50}$ titer to plaque

forming units (PFU), M is multiplied by 0.69[88]. This value is based on the Poisson distribution which calculates the probability of the number of viruses entering a cell, occurring in a fixed time interval and volume. Therefore, the probability (*P*) that a cell will become infected with *n* virions with a titer of *M* is 50% and can be calculated as follows:

General Poisson Distribution: Equation 3

$$P(n) = \frac{M^n \times e^{-M}}{n!}$$

$CCID_{50}$ predicts that at a certain volume of viral sample and over a certain amount of time, 50% of cells will be uninfected (n=0, P(n)=0.5)

$$0.5 = e^{-M}$$
$$-\ln(0.5) = M$$
$$0.69 = M$$

Therefore titer calculated from the $CCID_{50}$ overestimates the infectious titer by 31%, since 1 $CCID_{50}$ equates to approximately 0.69 plaque forming units. To correct for this, when one is calculating the MOI, the following equation is used:

$$MOI = \frac{0.69 \times M \times V}{C}$$ Equation 4

where:
C is the number of cells in the monolayer
M is the viral titer
V is the volume of diluted virus sample added to the monolayer of cells

This method is especially useful for viruses that are not able to form easily visible plaques such at canarypox. Additionally this assay is easier to perform than the plaque assay, although many replicates (at least 9) must be performed in order to increase the accuracy of this assay. The use of reporter genes or immunostaining against viral proteins[89] has been used to aid in the identification of CPE that is difficult to detect, which also increases the accuracy of this assay.

This method of infectious virus quantification suffers from similar problems as the plaque assay (technician bias and long incubation times), and thus this can slow the process optimization of a vaccine candidate.

2.3.3 Other Quantification Methods

2.3.3.1 Transmission Electron Microscopy (TEM)

A direct method of counting viral particles is by using TEM which allows scientist to visualize the viral particles and directly count the number of viruses. TEM passes a beam of electrons through a virus sample that has been negatively or positively stained in order to visualize the virus size or structure. The number of viral particles can then be counted by an operator and correlated to a viral titer. Although this method allows scientists to physically count the number of viral particles, the particles are not necessarily infectious, and this

method requires time consuming staining steps, along with expensive equipment and training[8].

2.3.3.2 Enzyme-Linked Immunosorbent Assay (ELISA)

ELISAs are a rapid method to determine levels of viral proteins and rely on the binding of viral antigens onto antibodies. In order to perform an ELISA, a specific antibody must bind to the target antigen and then a secondary detection antibody conjugated to horseradish peroxidase or alkaline phosphatase are used to label the primary antibody. A substrate will then be added which the enzyme cleaves in order to produce a colour change which can be measured using a spectrophotometer. The colour change can be compared to a calibration curve to quantify the amount of viral antigens in solution.

While this method is specific and rapid, it only measures the quantity of viral protein, which cannot be accurately correlated to an infectious viral titer or even a complete viral particle. In the case of subunit vaccines which consists of highly immunogenic viral proteins, such as the vaccine that contains gD protein mixed with adjuvant[90], an ELISA that uses antibodies against gD would be an effective method to measure protein concentrations. Many ELISAs are used to detect the presence of a virus in clinical samples due to their specificity and sensitivity.

2.3.3.3 Flow Cytometry

Previous work has identified flow cytometry as an appropriate tool for quickly and effectively estimating viral titer[12–15,21]. A flow cytometer passes individual particles single file through a beam of light, records the level of fluorescence or light scattering of the particle and has the ability to quantify thousands of particles per second that allows scientist to obtain a large sample size of a population. The large volume of data can then be used to analyze the physical characteristics of the particles based on the light scattering or fluorescence levels of the particles.

Most systems use fluorescence to detect infection either by using recombinant viruses that will cause a fluorescent protein to be produced by the cell or using immunofluorescent staining of viral glycoproteins on the surface of infected cells[16,91,92]. Systems have also been developed in which complementary cell lines harbor a gene for fluorescence that is activated once infected with a particular virus[17,18]. Although these methods can be used to accurately estimate infectious viral titer, they involve additional staining steps, which can have lengthy incubation times, as well as expensive reagents or require that stable mutants be created, a process that is labour intensive and time consuming. On the other hand, the granularity of cells, or intracellular complexity, has been previously reported to change during the course of infection for Sf-9 cells infected with baculovirus, HEK293 cells infected with a replication deficient adenovirus, and MNA cells infected with rabies[19,20,93]. This change in granularity can be measured using flow cytometry by observing the shift in side scatter (SSC) of an infected cell population[19,21].

2.3.3.3.1 Tracking Infection Using Fluorescence

Scientists have used fluorescent proteins in many different ways in attempts to measure and track the infection of cells. One of the methods is to stain viral proteins with a fluorescently tagged monoclonal antibody to confirm infection and then measuring the fluorescence of each individual cells by flow cytometry[15]. The population of fluorescent cells represents the number of successful infections and can be correlated to an infectious viral titer. This method can be prone to error if there is unspecific binding of antibodies, or if there is poor viral protein production in the cell.

Another method to obtain fast fluorescent readings is to insert a gene for a fluorescent protein into the virus that is expressed when the virus infects a cell[94,95]. This is a useful method to quantify infectious viral particles, but it requires the engineering of the virus, and may not be acceptable if the virus is the desired end product.

A further method for detection of infectious virus is to have a "reporter" cell line. Kung *et al.* have designed a Vero cell line for the detection of HSV by stably transfecting cells with a plasmid encoding the green fluorescent protein (GFP) under the control of the ICP10 promoter[17]. ICP10 (U_L39, called ICP6 in HSV-1) is a large subunit of the ribonucleotide reductase that is anchored in membranes and has protein kinase activity, but is nonessential and expressed in the early phase of gene expression (approximate 6-8 hpi)[37,96]. Kung *et al.* reported low levels of basal GFP expression in the Vero-ICP10-EGFP mutants, which would

make this an excellent reporter cell line to test clinical samples for HSV and as a rapid method to test the susceptibility of HSV antiviral drugs[97].

2.3.3.3.2 Tracking Infection Using Side Scatter

It is known that there is an increase in granularity of infected cell populations, but few articles attempt to explain or hypothesize as to why there is such an increase[19–21,93]. In flow cytometry, side scatter refers to the light that is scattered at large angles (15° to 150°) to the incident beam[98]. This bending of the light is commonly caused by granular internal structures within the cell. In the case of viral infection, this could be due to the restructuring of the host cell's cytoskeleton and organelles caused by the virus, or it could be caused by the additional viral components inside the cell. Increase in granularity has been noted in Sf-9 cells after infection with baculovirus, HEK293 cells infected with a replication deficient adenovirus containing the EGFP gene (Ad5GFP)[19–21]. A small increase in the population of MNA cells with high side scatter after 72 hpi with rabies virus has also been reported[93]. In Sf-9 cells infected with baculovirus, the side scatter could be correlated to recombinant protein production as well as monitoring the progression of baculovirus infection[19,99,100]. In adenovirus, the increase in granularity was found to be useful for the amplification of viral vectors, as the accumulation of viral genomes and viral proteins was thought to give rise to the increase in granularity in the cells[20].

2.3.4 Summary

The enumeration of viruses is a crucial step in the optimization of virus-based products. There exists a plethora of virus quantification techniques that each possess their own unique set of advantages and disadvantages which may limit their use (Table 2). Older methods such as the plaque assay and $CCID_{50}$ are traditional methods that are widely accepted, but these are simple methods that rely on the ability to visually detect signs of infection. Newer methods avoid the need of visual detection of CPE by employing dyes to stain viral components and sophisticated equipment to enumerate the number of cells which have been infected. The ideal quantification method would be rapid, sensitive and high throughput in order to aid in the optimization of viral production processes.

Table 2- Common viral quantification methods

	Plaque Assay	$CCID_{50}$	RT-qPCR Infectivity	Antigen Detection	Flow Cytometry	TEM
Time	5-9 days	5-12 days	1 day	3-5 hours	1 day	1 day
Sensitivity	High	High	Medium	High	Low	High
Measure	Infectivity, absolute	Infectivity, absolute	Genome relative	Antigen relative	Infectivity, absolute	Viral particles, absolute
Need of Standard	No	No	Yes	Yes	No	No
Specific Equipment	--	--	RT-PCR (expensive machine and reagents)	Spectrophotometer	Flow cytometer (expensive machine, cheap reagents)	Transmission electron microscope
Reproducibility	Low	Low	Excellent	Good	Excellent	Low
Cost	$	$	$$$$	$$$	$$$	$$$$
Human Labour	High	High	Medium	Medium	Low	High
Disadvantages	Prone to operator biases Time consuming Requires virus forms plaques	Time consuming Requires large number of replicates	Replication cycle dependent Difficult for viruses with high mutation rate	Cannot be extrapolated to an infectious viral titer Requires highly specific antibodies Difficult for viruses with high mutation rate (influenza)	Limited sensitivity Replication cycle dependent	Cannot be extrapolated to an infectious viral titer Time consuming staining Expensive equipment and staining reagents
Advantages	High sensitivity	High sensitivity	Rapid	Rapid	Rapid Very low variability	High sensitivity
Prerequisites	None	None	Primer choice PCR Settings Calibration of infectious units	Specific antibody must be available	Time of single viral infection cycle needs to be determined	Highly trained technician

Chapter 3

General Materials and Methods

3.1 Cell Lines and Virus

The HSV-2 viral stock used in this study was ACAM529, a monoclonal mutant that is replication-deficient in non-complementary cells due to the absence of U_L5 and U_L29 genes [101–103]. ACAM529 was stored at -80ºC, thawed in a 37ºC water bath immediately before use, and then diluted with ice-cold cell media prior to infection of HSV2013-121, HSV2012-121 or Vero cells (ATCC, Manassas,VA). HSV2013-121 is a complementing Vero cell line designed specifically to contain the U_L5 and U_L29 genes of HSV-2 missing from ACAM529. HSV2012-121 is a complementing Vero cell line that contains the U_L5 and U_L29 genes of HSV-2 as well as a GFP gene that is stably transduced under the control of a HSV-2 ICP10 promoter. All Vero-based cells were maintained in Dulbecco's Modified Eagle Medium (DMEM) with F12 (Corning Cellgro, Manassas, VA) supplemented with 10% heat inactivated fetal bovine serum (FBS) (Gibco Life Technologies, Burlington, Canada), and 4mM L-glutamine (Sigma-Aldrich, Oakville, Canada) at 37ºC in 5% CO_2 in T-flasks.

The ALVAC.gfp virus is a highly attenuate canarypox virus that contains a GFP gene as well as two HIV-1 genes (Gag and Env)[104]. ALVAC.gfp was stored at -80ºC, thawed in a 37ºC water bath immediately before use, and then diluted with ice-cold cell media prior to

infection of QT-35 cells (ECCAC, Salisbury, United Kingdom). QT-35 cells were maintained in Eagle's Minimum Essential Media (Sigma-Aldrich, Oakville, Canada), supplemented with 10% FBS (Gibco Life Technologies, Burlington, Canada), 1% Non-Essential Amino Acids (Sigma-Aldrich, Oakville, Canada), and 2mM L-glutamine (Sigma-Aldrich, Oakville, Canada).

All cultures were grown in surface tissue culture flasks (Thermo Scientific, Waltham, MA) with vented caps. The complementary GFP Vero (HSV2012-121), complementary non-GFP Vero (HSV2013-121) cells and ACAM529 and ALVAC.gfp were generously provided by Sanofi Pasteur.

3.2 Plaque Assay

Multiplicity of infection (MOI) for each experiment was determined by performing plaque assays with complementary non-GFP Vero cells. Cells were plated on 12-well tissue culture plates at a concentration of $3x10^5$ cells per well and incubated overnight. The next day, the cells were washed once with Dulbecco's Phosphate Buffered Saline (D-PBS) (Life Technologies, Burlington, Canada) and incubated with 200 µL of virus serially diluted in ice cold DMEM. The cells were incubated at 37°C for 1 hour, with gentle rocking every 15 minutes. After 1 hour, 1 mL overlay media (DMEM, 200mM L-glutamine, 10% heat inactivated FBS, 10% Penicillin/Streptomycin, 7.5% methyl cellulose) was added and the cells were incubated for an additional 48 hours. After incubation, the overlay media was removed and the plates were stained with a 300 µL of 1% crystal violet solution for 30

minutes. The crystal violet solution was removed, and the plate was rinsed with DI water and the plates were scored based on the number of visible plaques.

3.3 Infection of Cells Prior to Flow Cytometry

Complementary non-GFP Vero or complementary GFP Vero cells were plated onto 12-, 48- and 96-well plates at a concentration of $3.0x10^5$ cells/mL and incubated overnight. The next day, the spent media was aspirated using a vacuum pump and the cells were washed once with D-PBS. Virus samples were serially diluted in ice cold DMEM media just prior to infection. The cells were subsequently incubated with 200 µL, 100 µL or 50 µL of diluted virus for 1 hour to allow for viral particle adhesion and infection of the cells. After the incubation period, 1 mL, 200 µL or no cell culture media was added and the cells were incubated for an additional 0, 12, 16, 20, 24, 36, 48 or 72 hours.

3.4 Flow Cytometry

Following infection and detachment, cells were either filtered using a 40nm nylon mesh or treated with Accumax (Innovative Cell Technologies, San Diego, CA) and then exposed to 2% formaldehyde for 1 hour at 4ºC. Samples were then transferred into round bottom culture tubes (VWR, Mississauga, Canada) for flow cytometric measurements. A FACSCalibur flow cytometer (BD Biosciences, San Jose, CA) equipped with a 15 mW air-cooled argon-ion laser with an excitation frequency of 488nm, was used in this work. Full technical specifications of the flow cytometer can be found on the BD Biosciences website (http://www.bdbiosciences.com/documents/FACSCalibur_Flow__Cytometry_TechSpec.pdf).

Forward scatter (FSC) photomultiplier tube (PMT) voltage was 6.00 mV with the amplifier set to E01, side scatter (SSC) PMT voltage was set to 280 mV, the FL1 was set to 580 mV and, the FL3 was set to 800 mV. Samples were run for 10,000 events at the high flow setting (60 μL/min).

3.4.1 Data Visualization and Analysis

Data from the FACSCalibur flow cytometer was analyzed using FlowJo software (FlowJo, Ashland, OR). Initial gating was conducted on a SSC versus FSC scatter plot using cells that were not exposed to any virus to separate debris from whole cells. Three histograms were made based off the whole cell population; SSC, green fluorescence (FL1), and red fluorescence (FL3). For the SSC histogram, a gate was placed using a sample that was not exposed to virus such that the negative control contained 5% of highly granular cells. This gate was then applied to all samples. The count of events in the high granular region (the SSC-H+ region in Figure 7B) was used as an indicator of the cellular response to infection. To calculate the operating limits of the assay, the limit of detection (LOD) and limit of quantification (LOQ) were calculated based off the variance of the blank as described in references 32 and 33. Briefly, the LOD was calculated by adding $3*SD_{Blank}$ to the average of the blank (n=47) and LOQ was calculated by adding $10*SD_{Blank}$ to the average of the blank.

Chapter 4

Tracking Infection using Flow Cytometry

4.1 Chapter Objective

Flow cytometry has previously been shown as a viable tool in identifying and quantifying infection in cells such as baculovirus and adenovirus[19,20]. A flow cytometer has the ability to collect large amounts of data in a short amount of time which allows scientists to observe changes in cell populations and distinguish different populations based on side scatter, forward scatter and fluorescence markers. Here, flow cytometry is used to observe changes in the complementary GFP Vero and complementary non-GFP Vero cell lines after infection with a replication deficient HSV-2 virus (ACAM529). Each cell line contains the U_L5 and U_L29 genes that have been deleted from ACAM529, the complementary GFP Vero cell line additionally has a GFP encoding gene that is under the control of the ICP10 promoter which should be activated after infection with HSV-2.

The goal of these experiments was to identify the optimal parameter that could be correlated to the initial titer of virus by observing the levels of green fluorescence, side scattered light and forward scattered light using flow cytometry.

4.2 Materials and Methods

4.2.1 Cell Line and Virus

Complementary GFP Vero and complementary non-GFP Vero cells were maintained as previously specified and then plated onto 48-well plates, incubated overnight and washed once with D-PBS prior to infection with ACAM529. The infectious titer of the virus was calculated by using a plaque assay described in Chapter 3.

4.2.2 Flow Cytometry Sample Preparation

After the specified infection time, the wells were aspirated to remove the media and the remaining cells were treated with 200 μL trypsin and strained through a 40 nm mesh to remove cell clumps. The recovered cells were treated with an equal volume of 4% formaldehyde before being transferred to 5 mL polystyrene culture tubes and stored at 4°C for 1 hour. The final volume for a 48-well plate was 400 μL. After the cells were fixed, the samples were run through the FACScalibur using the settings described in Chapter 3.

4.2.3 ImageStream^{X} Mark II

Images and additional flow cytometry data were collected using an ImageStreamX Mark II (Amnis, Seattle, WA) equipped with 488 nm, 642 nm and 785 nm lasers, and a CCD camera with 20x, 40x, and 60x magnification potential. All images were taken with 40x magnification. To collect images of cells, gating was set before data acquisition using the INSPIRE (Amnis, Seattle, WA) software. Approximately 300 images were collected per

sample. The images and flow cytometer data were analyzed using the IDEAS software (Amnis, Seattle, WA) and final gating was completed as previously stated. Cell size was also calculated by the IDEAS software which measures the number of pixels in the mask applied to particle and then the number of pixels is converted to area in units of square microns.

4.2.4 Immunostaining

To confirm infection, $6.0x10^5$ cells were grown on 6-well plates overnight, washed once with D-PBS and infected. After 20 hpi, the media was aspirated and the cells were treated with trypsin for 10 minutes. The infected cells and uninfected control were stained for 1 hour at room temperature with 100µL of rabbit polyclonal anti-HSV-1 and HSV-2 antibodies (Abcam, Cambridge, MA; used at a 3:1000 dilution) washed two times using D-PBS, and then incubated for 1 hour with 100 µL of goat anti-rabbit IgG H&L Alexa Fluor® 647 (Abcam, Cambridge, MA; used at 3:1000 dilution). Samples were then transferred into round bottom culture tubes for flow cytometric measurements using the FACSCalibur flow cytometer and ImageStream^X.

4.2.5 Data Analysis

FlowJo was used to gate and analyze the flow cytometry data. Initially a gate was placed on the uninfected cells (blank) to identify the region with whole cells (Q2 region) based on the FSC and SSC scatterplot (Figure 7). Then the Q2 region of Figure 7A was used to make histograms of FL1 (green fluorescence) in Figure 7C, SSC (side scatter) in Figure 7B and FSC (Figure 7D). The gate for histograms was placed such that there was 2-%5% overlap

between the positive and negative regions (Figure 7). These gates were then applied to the infected samples for the respective time point.

For the FL3 histogram (Figure 7E), which was used to measure the amount of bound Alexa Fluor® 647, a gate was placed using a sample that was not exposed to virus such that there was 3% false positives for infection. The count of events in the high fluorescent region (H-FL3+) was used to confirm the number of infected cells based on immunofluorescent staining. The positive region from the FL3 histogram (FL3+) was then further gated using the gate from the SSC histogram. This was used to determine the level of granularity in infected cells.

A count was then taken of the number of cells that were in the positive (+) or negative (-) region of the gate. The number of cells or percent of the population in the positive region were plotted over time to determine trends in response when cells were exposed to various levels of virus.

[1]Wilcoxon rank sum was used to compare two distributions since they were non-normal. This test is a non-parametric hypothesis test used to compare two non-normal samples.

A. B. C.

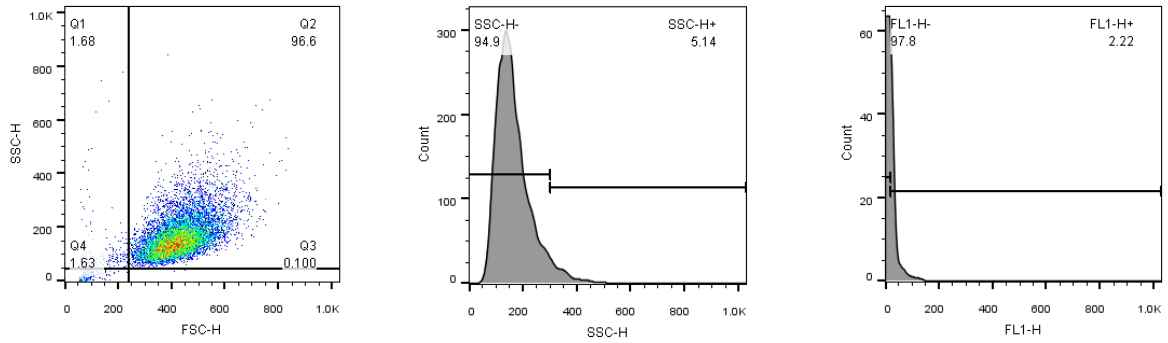

D. E.

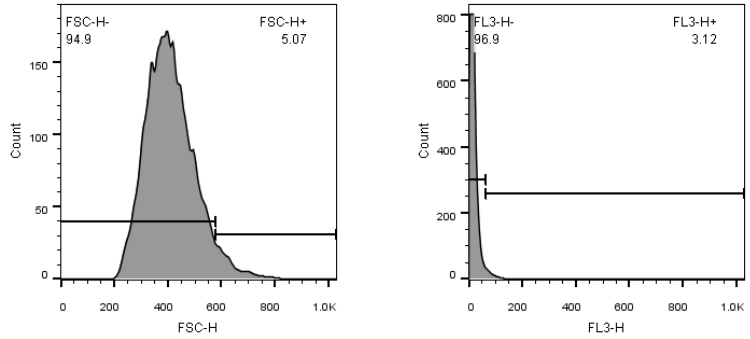

Figure 7-Sample gating on raw plots of uninfected complementary GFP Vero cells at 0 hpi

A. A scatter plot of FSC vs SSC was used to identify whole cells from cellular debris. The Q2 region from plot A was then used to make the histograms. B. A histogram of the side scatter values (SSC) for the Q2 population of an uninfected sample with a gate placed such that 5.14% of the population is in the highly granular region. C. A histogram of FL1 which measures the amount of green fluorescence of the Q2 population. D. A histogram of forward scattered light (FSC) of the Q2 population with a gate placed on the right end of the distribution that is set such that 5.07% of the population has a large amount of forward scattered light. E. A histogram of FL3 to demonstrate the red fluorescence of the Q2 population with the gate set so that 3.12% of the population has a high amount of red fluorescence.

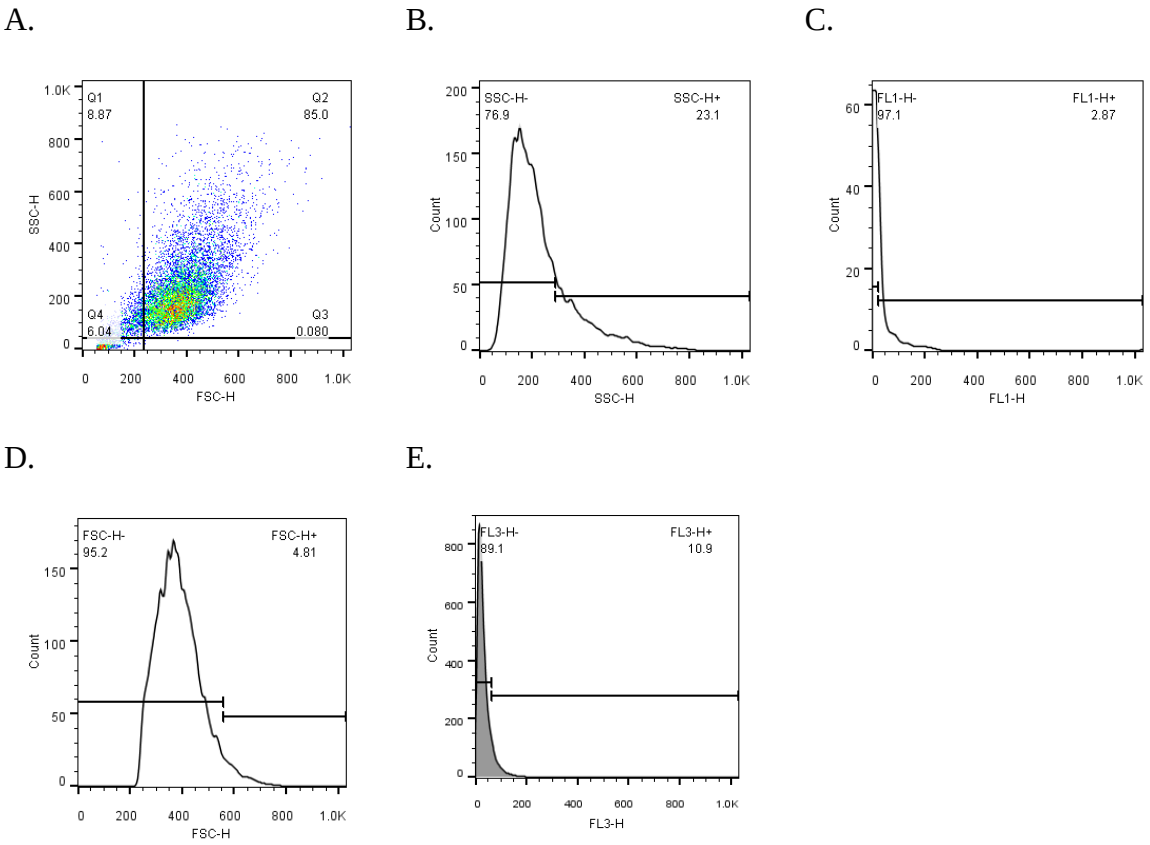

Figure 8- Sample gating on raw plots of infected complementary GFP Vero cells at 20 hpi

A. The gate from the uninfected cell population is applied to the infected cell population to remove cell debris. The Q2 region from plot A was then used to make the histograms. B. A histogram of the side scatter values (SSC) for the Q2 population of an infected sample with a gate made from the uninfected cell population. C. A histogram of FL1 which measures the amount of green fluorescence of the Q2 population. D. A histogram of forward scattered light (FSC) of the Q2 population with a gate from the uninfected population. E. A histogram of FL3 to demonstrate the red fluorescence of the Q2 population of an infected cell population that has also been stained from HSV-2 late structural proteins.

4.3 Results

4.3.1 Tracking infection of the complementary GFP Vero cells using FSC, SSC and FL1

Three different parameters were tracked over time (FSC, SSC and GFP) to observe the changes in the cells after they were exposed to various dilutions of virus. No increase in the forward scattered light could be observed as the infection progressed over 48 hours (Figure 9A). There was no significant increase in the FSC levels in any of the populations, instead the amount of cells in the population with a high amount of forward scattered light decreased over time.

Alternatively, the amount of cells with high levels of side scatter did increase with time, and increases could be seen as soon as 12 hpi (Figure 9B). After 12 hours, the percentage of cells with a high level of intracellular complexity increased with time. A significant difference can be seen between the various MOIs, although the lowest MOI of 0.005 was not significantly different from the uninfected sample even at 48 hpi. In fact, the number of cells with high granularity for the uninfected, MOI 0.005 and MOI 0.05 samples decreased over time.

Figure 10 demonstrates an increase in the number of cells with high levels of GFP over a 48 hour time period. After 8 hpi, there is no significant difference between the uninfected population (Blank) and the highest MOI of 5. It is not until 20 hpi that there is a modest increase in the number of cells that have a high level of GFP (8%). At the lower MOIs, there was no increase in GFP expression levels over 48 hours, which demonstrates a lack of

sensitivity of the ICP10 promoter in the cell line to demonstrate infection. Unlike the previous two parameters (FSC and SSC), there is no decrease in the basal level of fluorescence in any of the samples.

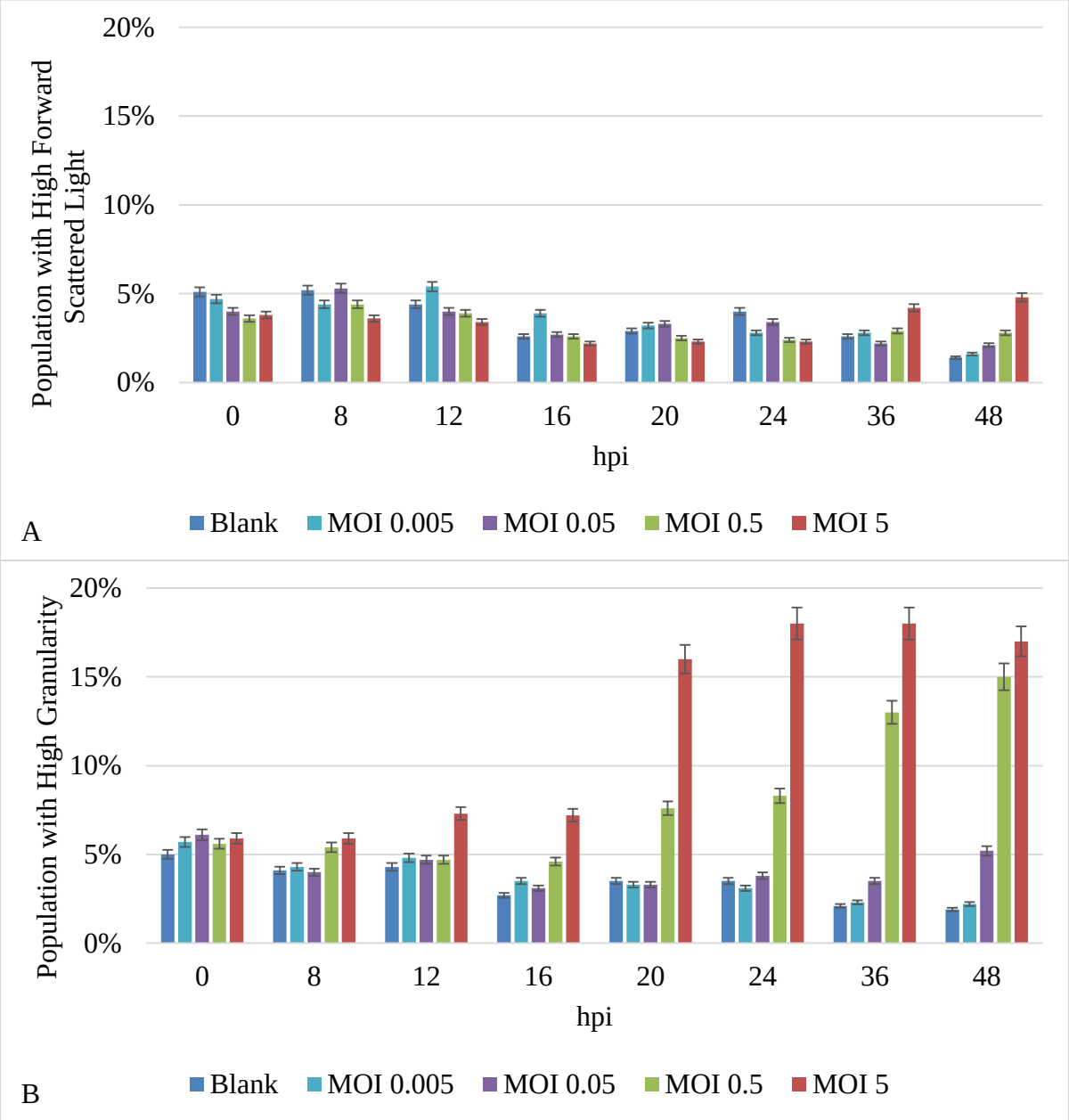

Figure 9- Forward scattered light and side scattered light levels in the complementary GFP Vero cells infected with ACAM529 tracked over 48 hours

A. The percent of the sample population that demonstrates high levels of forward scattered light (FSC) for 5 different MOIs (0, 0.005, 0.05, 0.5, 5). B. The percent of the sample population that demonstrates high levels of side scattered light (SSC) for 5 different MOIs (0, 0.005, 0.05, 0.5, 5).

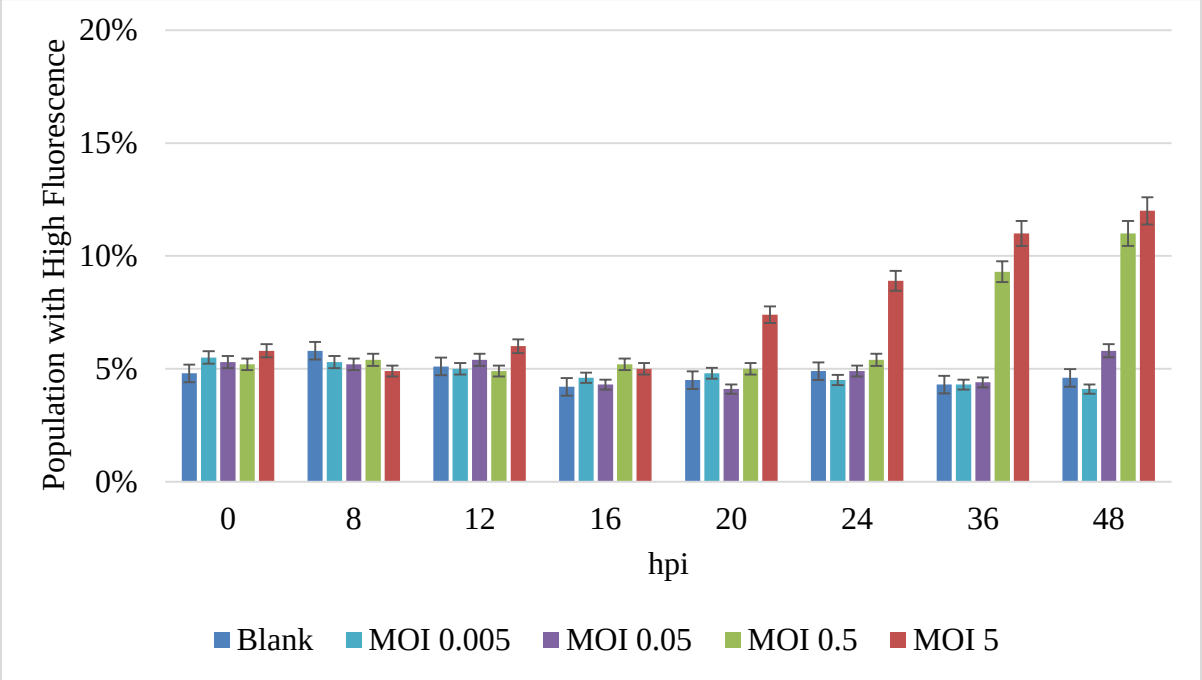

Figure 10-GFP levels in the complementary GFP Vero cells infected with ACAM529 tracked over 48 hours

The percent of the sample population that demonstrates high levels of green fluorescence for 5 different MOIs (0, 0.005, 0.05, 0.5, 5).

4.3.2 Tracking infection of complementary non-GFP Vero cells using FSC and SSC

To determine if the increase in side scatter was just an artifact of the complementary GFP Vero cell line, the complementary non-GFP Vero cells were infected with an MOI of 0.1 and the SSC and FSC values were measured over 36 hours. Figure 11A visually demonstrates the progression of the infection of the cells over 36 hours. During the first 12 hours of infection, little CPE can be observed. At 20 hpi, it can be seen that syncytial cells are forming along with cell rounding and detachment. At 36 hpi, the entire culture is infected, which shows that the virus has spread to all the surrounding cells. Similarly, these changes can be observed in the SSC histograms, where an increased CPE correlates to a shift of the cell population to greater SSC values (Figure 11B). There was no change in the median of forward scatter values of the cells, which would indicate that the relative opaqueness of the cells remains relatively constant throughout the infection. The gates for Figure 11B&C were placed such that 5% of the uninfected population would have a high SSC or high FSC score. The gate provides a threshold that distinguishes between cells that have a high enough level of granularity to be considered ‘infected’ and cells that are ‘uninfected’.

In order to compare the complementary GFP Vero cells and complementary non-GFP Vero cells, a time course over 48 hours was conducted under the same conditions as with the complementary GFP Vero cells and similar results were seen (Figure 12). The number of cells with high granularity increased with increasing MOI and time, until 48 hpi where the cells infected with an MOI 5 or MOI 0.5 had approximately the same number of cells with high granularity. A significant difference can be seen between MOIs as early as 12 hpi in the

SSC plot and at 20 hpi in the FSC plot. From 20 to 24 hpi, there was no change in the amount of cells that displayed high granularity for MOI 5, this plateau is also seen in the FSC graph (Figure 12B). At 36 hpi, both parameters (FSC and SSC) reach a maximum and a decline is seen at 48 hpi.

In order to validate that these results are not an artifact of a single flow cytometer, another flow cytometer (ImageStream^X) was used to measure the granularity of infected cells at 20 hpi. In addition to granularity, the cell size was also investigated. It was found that there was an increase in both the number of cells with a large cell size and increased granularity post-infection (Figure 13). The large cells appear to increase the range of distribution of the histogram and the 'large cell' events appeared more likely to be clumps of cells, instead of large single cells. To test if the granularity is linked to large cell clumps, the granularity of each event was divided by the cell area (High Average Granularity). The cells with high average granularity are marked in teal on the histograms for cell size and side scatter (Figure 13B). It can be seen these cells all have high granularity, but their sizes vary greatly, indicating that granularity is not necessarily linked to cell size.

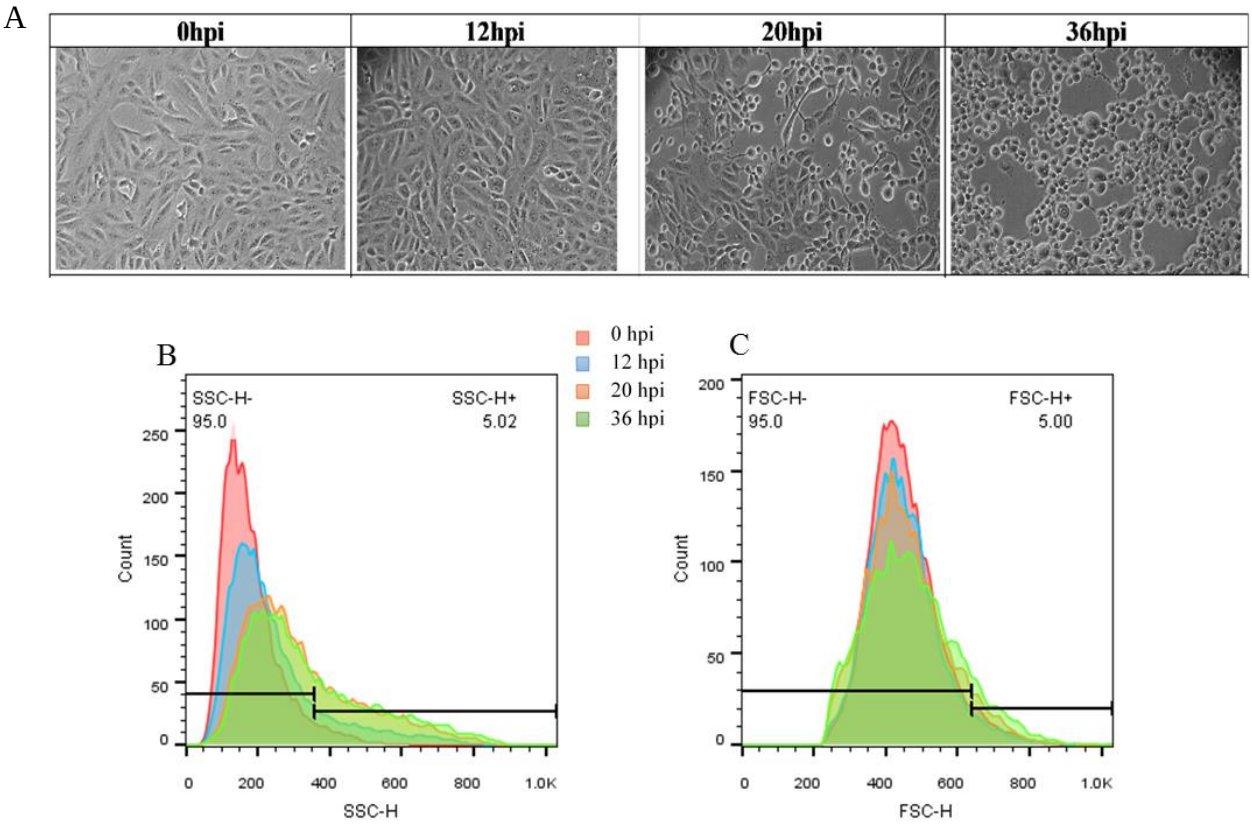

Figure 11- Complementary non-GFP Vero cells were infected at an MOI of 0.1 over 36 hours

A. The progress of the infection under 10x magnification. B. A histogram of SSC that shows the general increase in granularity overtime. C. The histogram of FSC for the cell population over time.

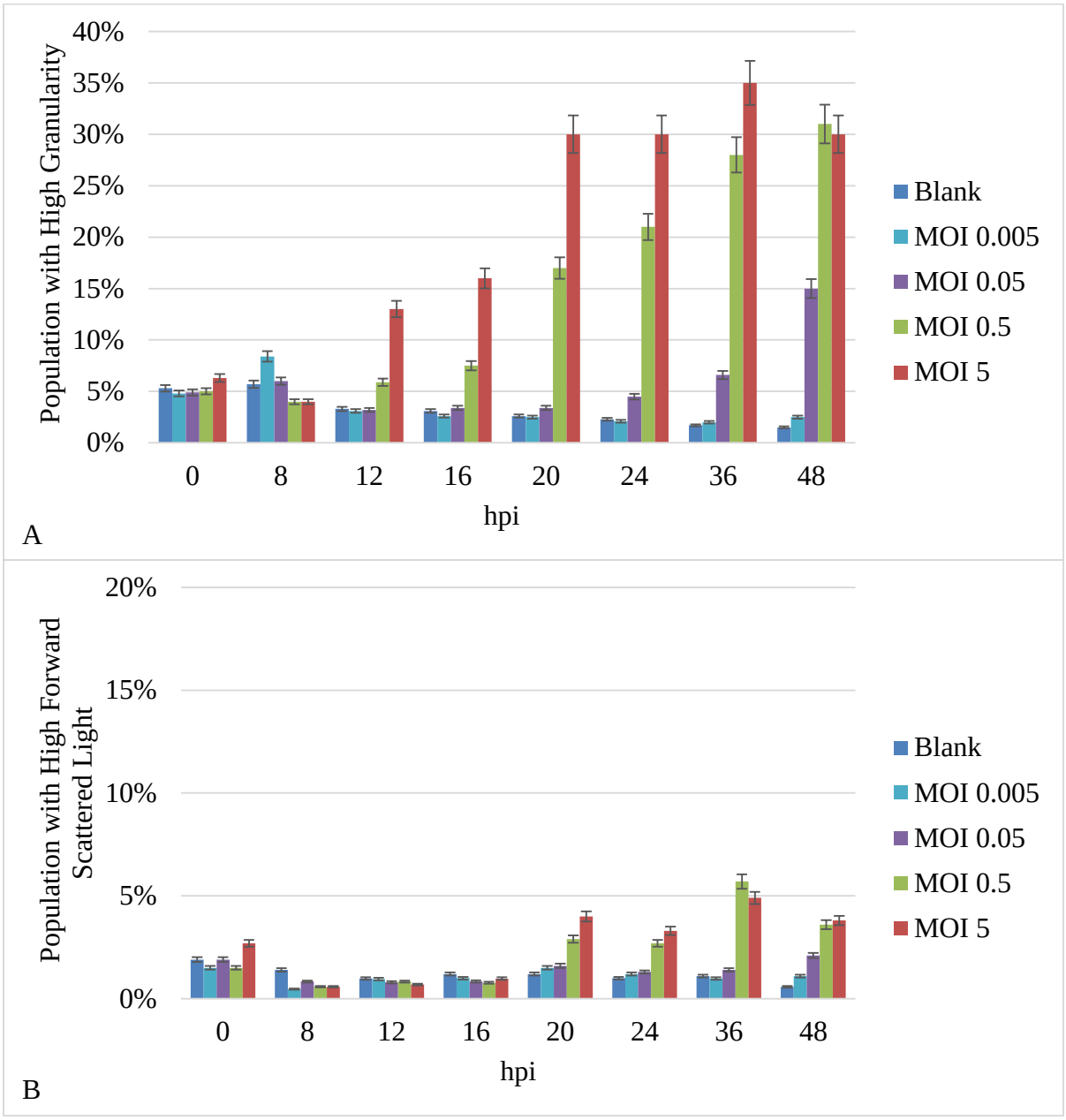

Figure 12- FSC and SSC levels in complementary non-GFP Vero cells infected with ACAM529 tracked over 48 hours

A. The percent of the sample population that demonstrates high levels of side scattered light (SSC) for 5 different MOIs (0, 5, 0.5, 0.05, 0.005). B. The percent of the sample population that demonstrates high levels of forward scattered light (FSC) for 5 different MOIs (0, 5, 0.5, 0.05, 0.005).

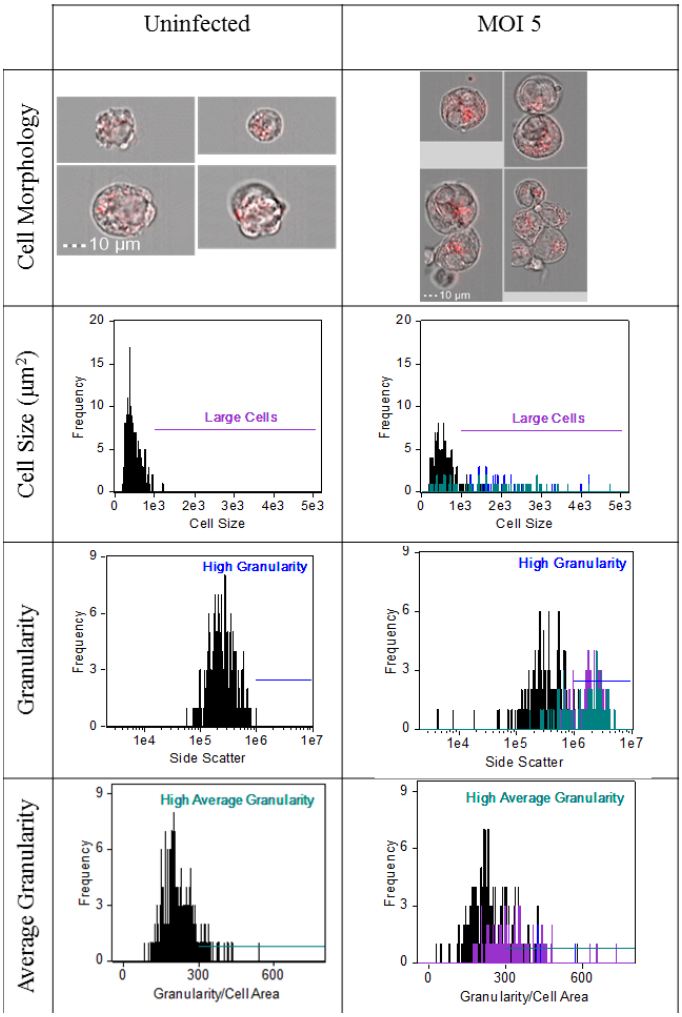

Figure 13- Cell size and granularity comparison for complementary non-GFP Vero cells

Complementary non-GFP Vero cells were infected with a MOI of 5 or mock treated with media containing no virus. The samples were fixed after 20 hpi and the cells size (μm^2), granularity and average granularity per cell area were calculated using the ImageStream^X.

4.3.3 Evidence indicating granularity caused by infection and replication

To support the idea that the increase in granularity of cells is caused by successful infection and viral replication, cells were stained for viral proteins for an infected cell sample (MOI 25) and an uninfected cell sample (Uninfected) (Figure 14). Infected cells were tagged using an antibody against HSV1/2 late structural proteins and then the antibody was stained using an Alexa Fluor® 647 to determine if the cells had been successfully infected. The cells that were successfully infected should have produced late structural viral proteins and therefore should have had high levels of red fluorescence due to the staining. The curves for the histogram were determined to be non-normal, therefore the medians were compared using the Wilcoxon rank sum test[1] to determine significant differences between the populations. It was found that there was a significant ($p<0.001$) difference in the median granularities between the positively and negatively stained cells (FL3+ and FL3-). The infected cell population (FL3+) had a higher median for the SSC than the uninfected samples. There appears to be a small subset of cells in the infected sample that had a low amount of fluorescence, indicating that they were not infected or that they had not produced adequate amounts of late structural proteins at 20 hpi.

As another means to assess if the increase in granularity is caused by successful replication of the ACAM529 virus, non-complementary Vero cells (cells do not contain HSV-2 U_L29 or U_L5 genes) were infected. After 20 hpi, it was found that there is no significant difference for MOIs below 0.5 and that the increase in granularity is much smaller than that seen using the

complementary non-GFP Vero cells which do include the U_L29 and U_L5 HSV-2 genes (Figure 15).

To ensure that the increase in granularity is not caused by other factors in the virus sample, such as cytokines or other cell signaling molecules, the virus was removed from solution through 0.1 μm filtration and the cells were exposed to the virus-free solution. The virus-free solution maintained approximately the same level of highly granular cells as the Blank sample over 48 hours of incubation (Figure 16). Samples infected with virus-containing solution showed an increase in the number of cells with high granularity over time.

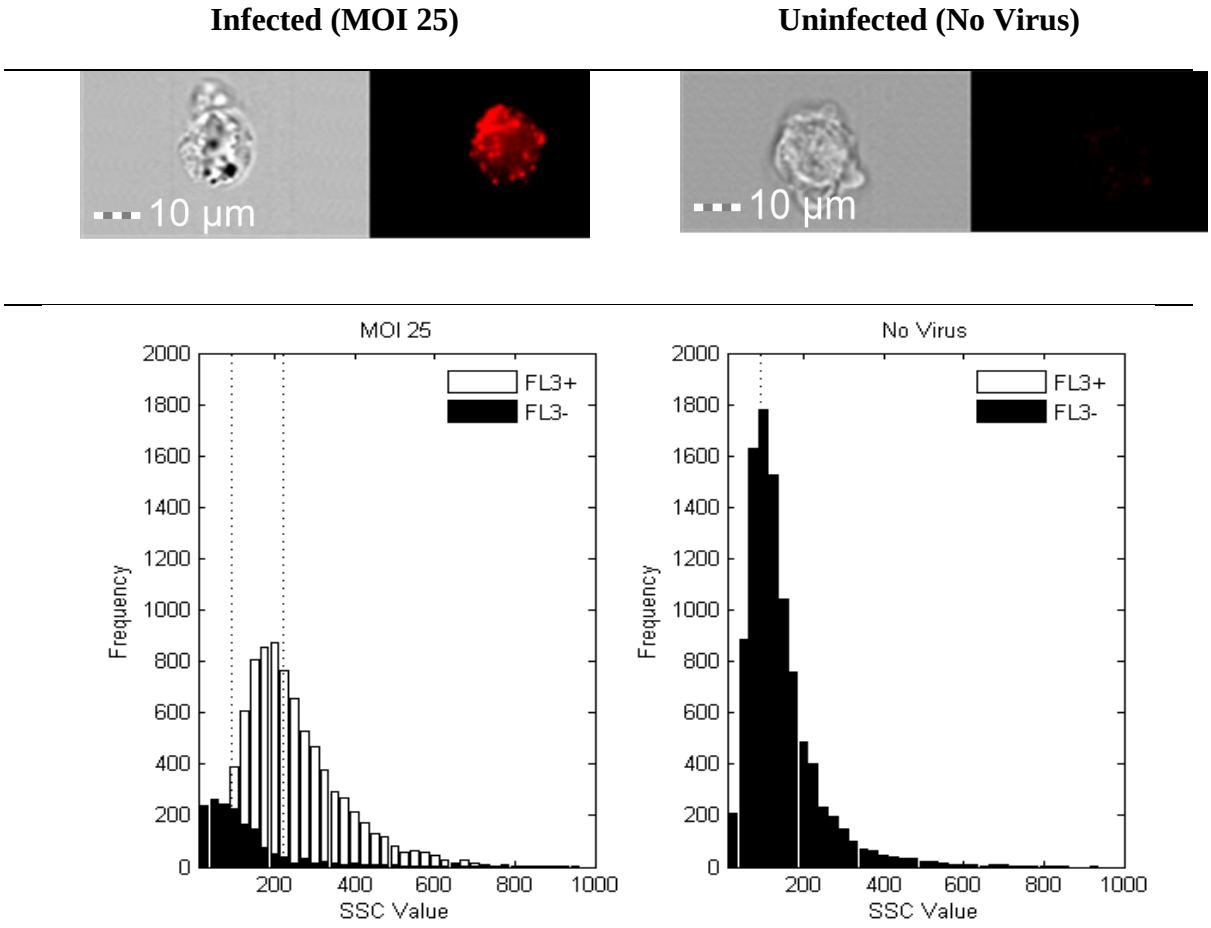

Figure 14- Granularity of infected cells and immunostained cells

Complementary non-GFP Vero cells were infected at an MOI of 25 or 0, incubated for 20 hpi and stained using an HSV-1/HSV-2 late structural protein primary antibody and Alexa secondary antibody to identify infected cells. The samples were then run through the flow cytometer to analyze their granularity. The infected cells were identified based on the amount of red fluorescence (FL3+) as compared to the fluorescence of the stained MOI 0 sample. The median of the infected (FL3+=222 IU) and uninfected (FL3-=93.5 IU) samples are significantly different (α=0.001, $p<0.001$), as well as the median of the infected (FL3+=222 IU) and MOI of 0 (119 IU) (α=0.001, $p<0.001$), as calculated by the Wilcoxon rank sum test.

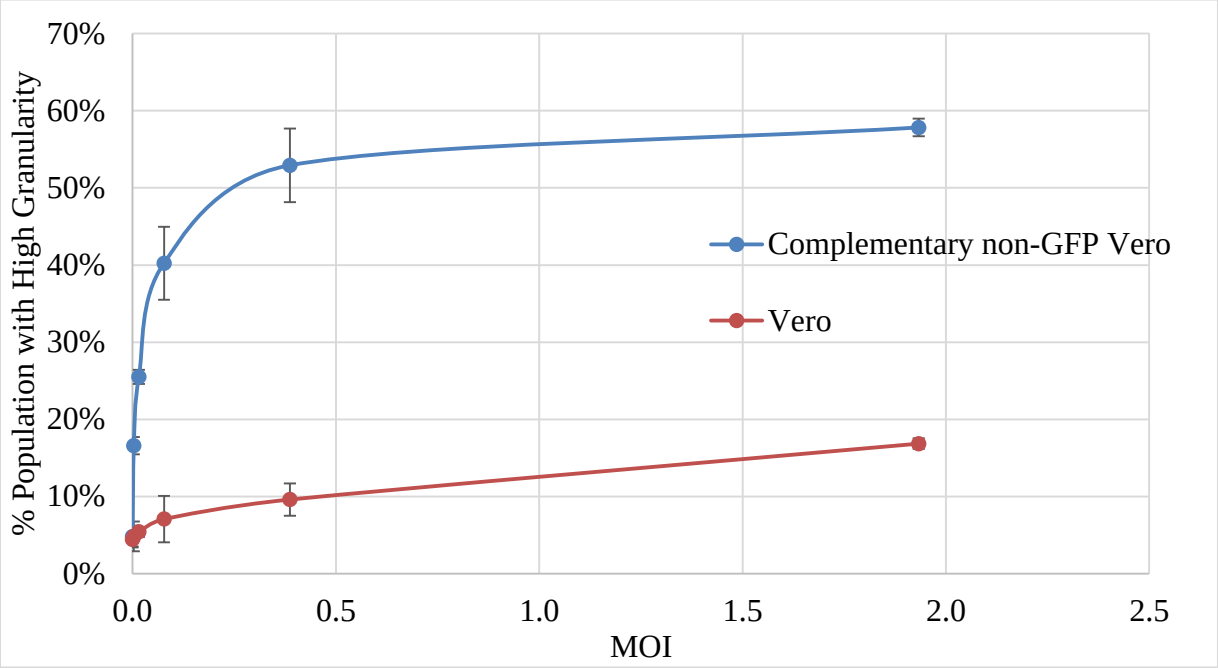

Figure 15- Granularity of Vero cells at 20 hpi

Non complementary Vero cells (Vero) and complementary non-GFP Vero cells were infected with 5 different concentrations of ACAM529 for 20 hpi in triplicate to assess the levels of granularity (SSC) of the cells. Error bars are one standard deviation and the experiment was conducted three times.

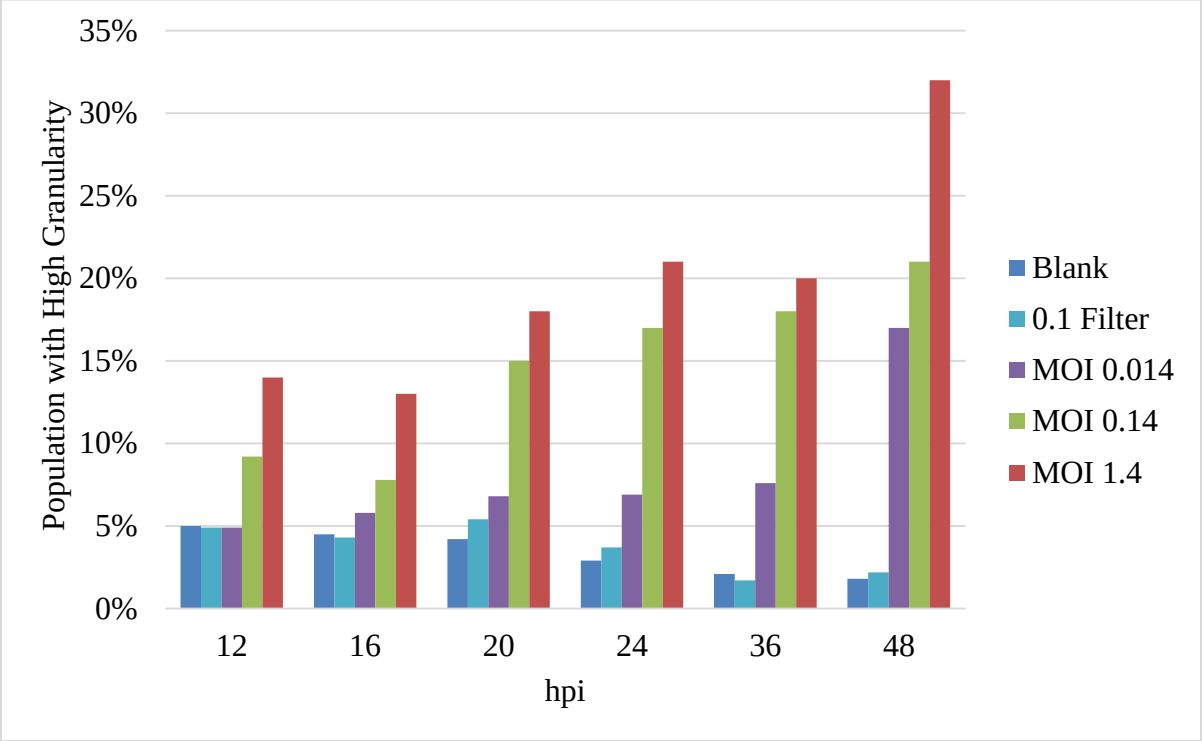

Figure 16 Complementary non-GFP Vero cells infected with supernatant of virus sample

Complementary non-GFP Vero cells were infected with a sample of virus that had been passed through a 0.1 μm filter to remove any viral particles from the solution. The cells were then exposed to the filtered supernatant for 20 hours. As a comparison, cells were also infected with 3 different dilutions of an unfiltered virus sample.

4.4 Discussion

ACAM529 infection induced a continuous increase in green fluorescence and cell granularity in the complementary GFP Vero cells as well as increased granularity in the complementary non-GFP Vero cells. To confirm if physiological changes could be used as a robust criterion for quantifying the ACAM529 virus, a combination of microscopy and flow cytometry were evaluated.

4.4.1 Identifying indicators for infection

The complementary GFP Vero cell line contains a GFP gene under the control of the ICP10 promoter from HSV-2. The promoter has a maximum expression 6-8 hpi. It was found that there was no discernable difference between infected samples until 20 hpi (Figure 10). The lack of the increase in the GFP signal could be due to a large amount of noise due to basal levels of GFP expression in uninfected cells coupled with weak expression of GFP in infected cells which masks the signal of the GFP produced due to infection. It was previously described by Kung *et al.* with a Vero-ICP10-GFP reporter cell line that a significant GFP signal could be detected as early as 6 hpi and with a large level of expression after 48 hpi[17]. Our data did not show significant difference until 20 hpi, with a maximum level of expression at 48 hpi. The high levels of basal GFP expression seen in our work is most likely due to the activation of the ICP10 promoter by activator protein 1 (AP-1) in the complementary GFP Vero cell line. ICP10 is the only HSV promoter that has AP-1 *cis*-response elements[107]. AP-1 refers to many heterodimeric transcription factors composed of

Jun, Fos or activating transcription factor (ATF) subunits that bind to common DNA sites to regulate gene expression in response to cytokines, growth factors, stress and viral infections[108]. Zhu and Aurelian found that basal expression of chloramphenicol acetyltransferase (CAT) under the control of the ICP10 promoter in Vero cells was significantly higher with 10% serum than with 0.5%[108]. In our studies, 10% FBS was used to maintain the cell line which would have increased the basal level of GFP expression. Zhu and Aurelian also found that there were low levels of expression in F9 cells which lack AP-1 transcriptions factors, compared to Vero cells which have some endogenous AP-1 (even with 0.5% serum levels)[108]. This indicates that the use of the ICP10 promoter in a Vero cell line was a poor design choice when the complementary GFP Vero cell line was created due to the endogenous expression of AP-1 transcription factors in Vero cells, and that basal expression of GFP is to be expected.

Due to the high levels of basal expression and the slow response time of the ICP10 promoter (20 hours), the change in SSC was seen as a more viable indicator of infection. Furthermore, tracking the number of cells with increased side scatter required a shorter incubation time to observe a significant difference (12 hpi) (Figure 9). At 20 hpi, the percent of cells with high granularity infected with an MOI of 5 was 3.5 times greater than the uninfected population, compared to the GFP levels which was only 1.5 times higher than the uninfected cells. The granularity only increased in cells that were exposed to virus. Because of this, the complementary non-GFP Vero cell line, which does not contain a reporter protein, was tested to determine if the same trend in granularity could be observed after infection.

It was found that the same trend occurred with the complementary non-GFP cell line, which indicates that the increase in granularity is not dependent on the ICP10-GFP genes. There was an increase in the right side of the distribution of cells with high SSC values overtime which correlates with the CPE that can be seen in the microscope images (Figure 11). This supports the idea that successful infection and viral replication in the cell gives rise to the increase in the intracellular complexity. At 36 hpi, it can be seen that almost all of the cells display CPE, while at 20 hpi there still appears to be some cells with healthy morphology (Figure 11). Conversely, the SSC histograms for both 20 and 36 hpi are almost identical, signifying that there exists a maximum number of cells that have high granularity in the population. This maximum value could be due to an equal number of cells being lysed from infection, and therefore not recorded, and the number of cells that are reaching the final stages of infection. Since the infection is not synchronous, or occurs at the same time for all cells, it is likely that the viruses are at various stages of their infection cycle at any one time. For example, a subset of virions could infect within the first 30 minutes of being exposed to cells, while other virions could take up to 2 hours to successfully enter the cell and begin replicating.

Regardless of the maximum number of cells with high granularity achieved, 36 hpi appeared to be the time point when the maximum is reached for both the GFP and non-GFP complementary Vero cells. The maximum percent of the population with high granularity was 17% for complementary GFP Vero cells and 35% for complementary non-GFP Vero cells. The discrepancy between the two cell lines could be due to the additional GFP

encoding gene under the control of the ICP10 promoter in the complementary GFP Vero cells. The additional burden on the cell to produce GFP could pull resources away from the production of the granular structures. The complementary non-GFP Vero cells do not have this burden; therefore, less of the cellular resources are being channeled away from the cause of the increase in granularity. To maximize the number of cells that display high levels of granularity, the complementary non-GFP Vero cells are used in further quantification experiments.

4.4.2 Evidence indicating granularity caused by infection and replication

To confirm that the cells which display CPE are in fact the cells that have high granularity, cells were stained for HSV-2 late structural proteins at 20 hpi and their granularity was compared to an uninfected sample (Figure 14). It was found that the medians were significantly different for the two non-normal distributions. The cells which stained positively for viral structural proteins had a distribution curve with a long right tail which was the same trend observed in the histograms seen in Figure 11B. The histogram for cells infected with an MOI of 25 also shows a small population of cells that do not have late structural HSV-2 proteins, this is mostly likely due to a non-synchronous infection, where the virus has not reached the late (γ) phase of gene expression which occurs after 15 hpi. This experiment demonstrates that there is significant difference in the average level of granularity in infected cells as opposed to uninfected cells. To verify that this response was not caused by cytokines or other cell signaling molecules in the supernatant of the virus sample, a viral sample filtered with a 0.1 μm filter was exposed to cells (average diameter of HSV-2 is 150

nm). It was found that there was no significant difference between the filtered sample and the uninfected sample demonstrating that the factors present in the viral media did not induce an increase in granularity in the cells (Figure 16).

As a final measure to ensure that the increase in granularity was caused by infection of the cell, Vero cells that do not contain the U_L29 and U_L5 HSV-2 genes were infected. It was seen that there was no increase in the number of cells with high granularity with increasing MOI at 20 hpi. Since ACAM529 cannot successfully replicate in Vero cells that do not contain the missing genes, very low levels of viral proteins can be expressed by the cell (Figure 15). This indicates that the successful replication of the virus in cells is one of the factors that causes the increase in granularity.

From these last set of experiments, there is strong evidence to support the idea that the increase in granularity is caused by the infection and replication of ACAM29 in complementary non-GFP Vero cells.

Chapter 5

Modelling Increase of Side Scatter

5.1 Chapter Objective

The objective of this series of experiments was to determine the best sampling time that will yield the most accurate and consistent results for predicting the initial titer of the virus stock solution. To evaluate this, a 72 hour time course was used to identify the key time points during the first phase of infection. The results were analyzed and the correlation between the MOI and percent of population with high granularity was established. The motivation for these experiments was to determine the shortest and most convenient incubation time to establish an accurate infectious titer.

5.2 Materials and Methods

5.2.1 Cell Line and Virus

Complementary non-GFP Vero cells were maintained as previously specified and then plated into 48-well plates and infected as previous stated in Chapter 5. The infectious titer of the virus was calculated by using a plaque assay.

5.2.2 Flow Cytometry Sample Preparation

After the specified infection time, the wells were aspirated and the cells were treated with Accumax to prevent cell aggregates. Once the cells were detached, an equal volume of 4% formaldehyde was added to the wells for a final volume of 400 μL and then the sample was transferred in to 5 mL polystyrene culture tubes and stored at 4°C for 1 hour. After the cells were fixed, the samples were run through the FACScalibur with the settings described in Chapter 3.4.

5.2.3 Data Analysis

Data was analyzed as described in Chapter 3.4.1.

5.3 Results

To determine the optimal sampling time to measure the side scatter, a 72 hour time course was conducted to study the effect of virus exposure on the granularity of the cells. In Figure 17, the infection of complementary non-GFP Vero cells using various MOIs was tracked over time.

As it can be seen, the amount of cells with high granularity increases dramatically from 0 to 16 hpi, where after from 16 to 20 hpi a plateau can be seen for all the viral dilutions. As the second round of infection begins after 20 hpi, it can be seen that there is another sharp increase in the number of cells with high granularity from 20 hours to 36 hours where the three highest MOIs reach the same maximum point at 36 hours (56%). The number of cells with a high amount of granularity decreases after 36 hpi, most likely due to cell death. The lowest MOI of 0.05 does not follow the same trend as the other three MOIs, it peaks at 48 hpi and then declines. This is most likely because the low amount of virus initially added, required more replication cycles to produce enough virus to infect the entire population of cells.

Since we are interested in the relationship between MOI and the percent of the population with high granularity, each time point was individually plotted (Figure 18). A logarithmic trend can be seen prior to 36 hpi in Figure 17. Therefore, the data was fitted to the logarithmic model:

$$\%\ cells\ with\ high\ side\ scatter = b_2 \ln MOI + b_1$$ **Equation 5**

Prior to 24 hpi, the R^2 value of the fitted model remains above 0.93 which demonstrates that the model is a good fit for those time points. It is not until 24 hpi where the slope (b_2) begins to decrease, and the R^2 value drops below an acceptable level (0.9). Therefore, the time points 16-22 hpi were chosen for more in depth analysis since they had the best fit to the model (R^2=0.95). Four time points were chosen (16, 18, 20 and 22 hpi) and 8 different viral dilutions were used to test the relationship between granularity, time and concentration of virus (Figure 19). It was found that at 22 hpi the R^2 value was below 0.9 indicating that the model is not a good fit for time points past 20 hpi.

The constants from Equation 5 (b_1 and b_2) both increased over time until after 20 hpi, where b_2 decreased (Table 3 andTable 4). For the two different trials seen in Figure 18 andFigure 19, the values for b_1 and b_2 were very different, even though the same type of cells, media and virus from the same bioreactor run were used. This indicates that there are some other factors that are not being controlled during the experiment that affects the response from the cells.

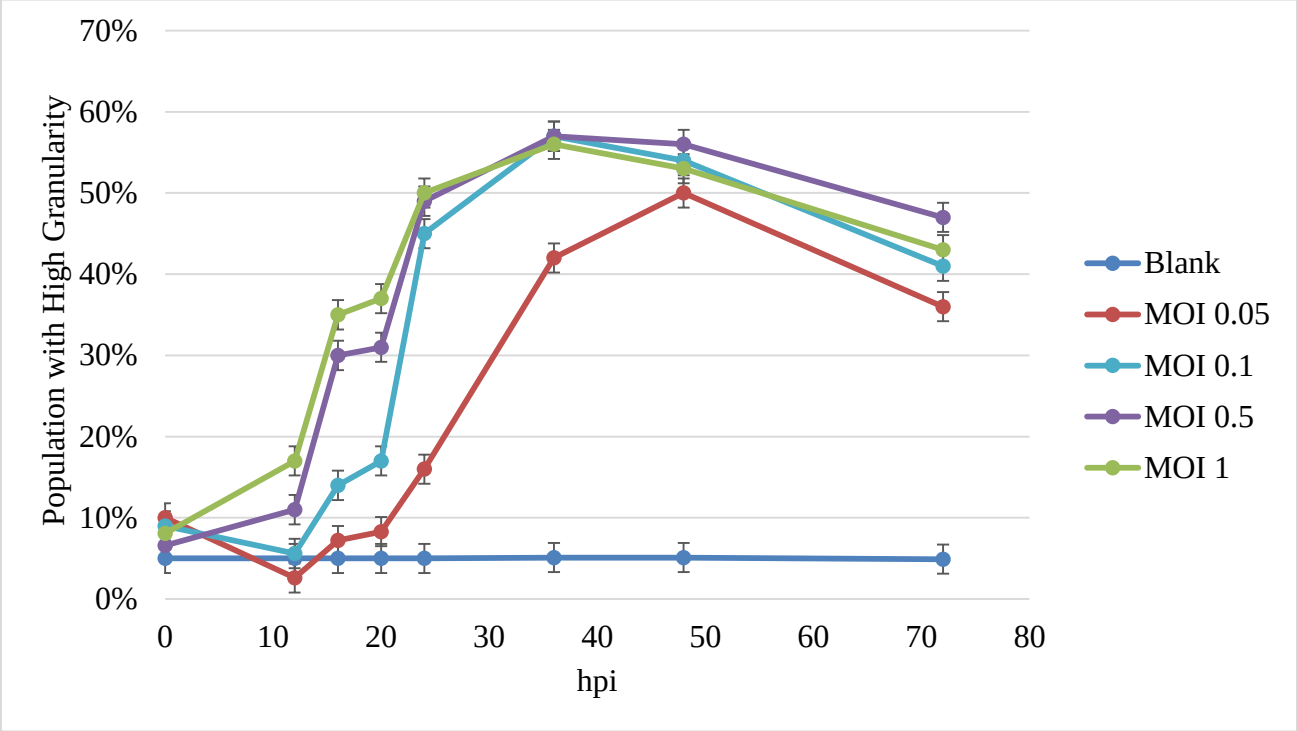

Figure 17- 72 hour time course of infection of the complementary non-GFP Vero cells with 5 different viral dilutions

Cells were plated onto 48-well plates overnight before being treated with viral dilutions corresponding to MOIs of 0, 0.05, 0.1, 0.5 and 1 at time points 0, 12, 16, 20, 24, 36, 48, 72 hpi. Error bars are the standard deviation of the blank over 72 hours.

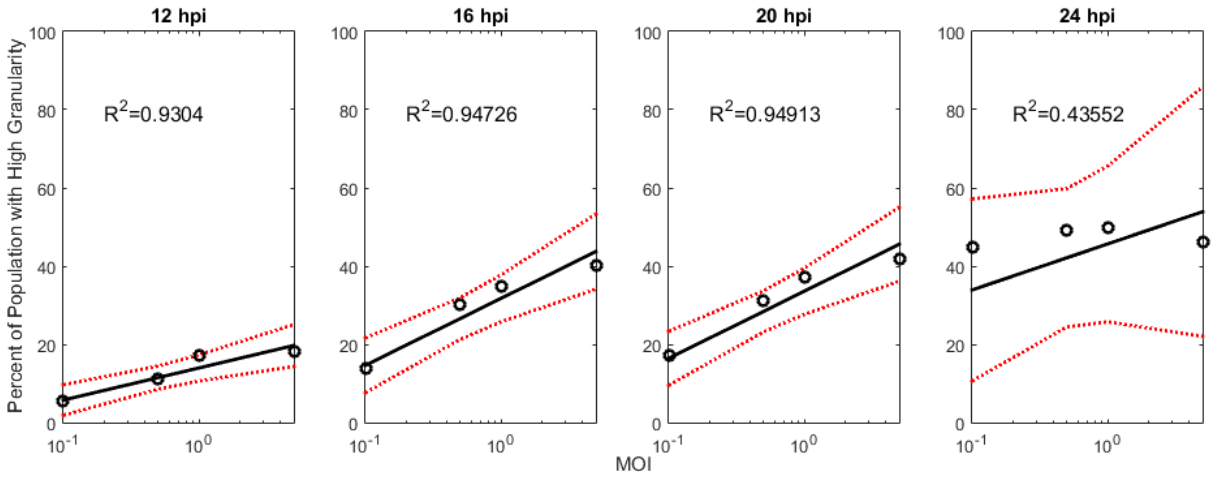

Figure 18- 72 hour time course data fitted to semi-logarithmic model demonstrating a direct relationship between the logarithm of MOI with the fraction of cells displaying high granularity

The data points (‘o’) are plotted on a semi-logarithmic axis for a single time point with the fitted model (Equation 5, solid black line) and a 95% confidence interval (dashed red line). There is a direct correlation between the logarithm of the MOI and the fraction of cells with high granularity prior to 24 hpi.

Table 3- Values of the b_1 and b_2 constants calculated for Equation 5 for 12-24 hpi.

The table displays the values for the constants (b_1 and b_2) at each time point from Figure 17, along with the R^2 value.

hpi	b_2	b_1	R^2
12	0.04	0.14	0.93
16	0.07	0.32	0.95
20	0.07	0.34	0.95
24	0.05	0.46	0.44

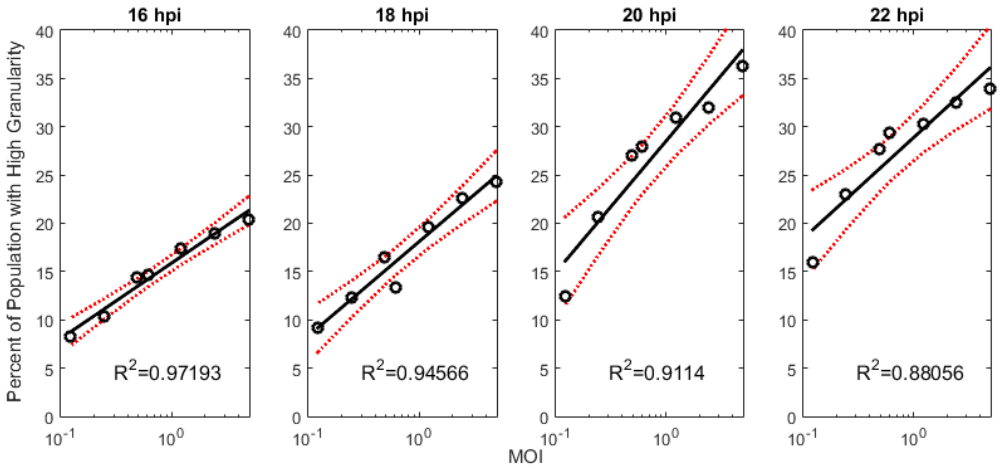

Figure 19- Correlation of MOI to fraction of the population with high granularity at 16, 18, 20 and 22 hpi

The data from each time point are plotted on a semi logarithmic plot to demonstrate the direct correlation with logarithmic trend lines. The error bars are the standard deviations obtained from triplicates.

Table 4- Values of the b_1 and b_2 constants calculated for Equation 5 for 16-22 hpi.

The table displays the values for the constants (b_1 and b_2) at each time point from Figure 18, along with the R^2 value.

hpi	b_2	b_1	R^2
16	0.03	0.16	0.97
18	0.04	0.18	0.95
20	0.06	0.29	0.91
22	0.05	0.29	0.88

5.4 Discussion

The assessment of the 72 hour time course study revealed that there is a maximum percent of cells in the population that have high granularity at 36 hpi. This peak corresponds to 100% CPE which was previously seen in the microscopy study (Figure 11A), indicating that all the cells in the well have been infected. This is most likely caused by a second round of infection which produced enough virus to spread to the entire culture. Since all the cells in the well have been infected at that time, later time points will only track the death of the population. This time point also exposes that all the MOIs are indistinguishable from each other at 36 hpi. For future assays, sampling times should occur before this time point to avoid inconclusive results.

The time points from 0 hpi to 20 hpi demonstrate a logarithmic trend, and prior to 24 hpi displayed a good fit using a logarithmic model (Figure 18). The 16 hpi to 20 hpi time points correlate when viral assembly occurs and viruses begin to travel to the basolateral side of the cell or tight junctions between cells, in preparation to exit the cell to begin a second round of infection. This plateau could be when the virus halts the replication of its components[37], and begins to assemble itself. Sandhu *et al.* theorized that the rise in granularity of HEK293 cells after infection with adenovirus is due to the accumulation of viral genomes and viral particles[20], which matches what is being observed with ACAM529 infection of the complementary non-GFP Vero cells. It is probable that the accumulation of ACAM529 components in the cells attribute to the increased levels of intracellular complexity that is being observed prior to 16 hpi. Azizi *et al.* demonstrated through RT-qPCR that the cycle

threshold value could be correlated with the logarithm of the infectious viral titer of ACAM529 for gD gene, but not for the ICP27 gene or thymidine kinase gene from 6 hpi to 20 hpi[9]. This provides some evidence that the rise in granularity in our work could be due to the accumulation of late expressed genes. After 20 hpi, a correlation could no longer been seen with the gD gene[9] or in granularity. This is most likely caused by progeny viruses infecting new cells which would increase the granularity in newly infected cells from 24 hpi to 36 hpi.

A closer look was taken at the 16 to 20 hpi time range to obtain more detailed results. It was found that the model yields a satisfactory fit for 16, 18 and 20 hpi, while 22 hpi proved to have a less good fit. The R^2 value decreased for 22 hpi which indicates that there is less of a correlation between the number of cells with high granularity and MOI. This supports the hypothesis that after 20 hpi the virus has stopped replicating itself and exits the cell to begin a second round of infection[17]. This study also demonstrates the large difference between the time points 16, 18 and 20 hpi. The addition of 2 hours between the time points reveals a large difference in the values for the constants in the model. This highlights the importance of infecting the entire 96-well plate in the shortest time possible. If the first and last well are infected 2 hours or more apart, the sampling time for the plate will not be a constant, and the model equation will have to take into account variable time and MOI. Thus, in order for the assumption of constant time to be made, all samples must be platted within 2 hours (or less) of each other.

Given that the constants for the model depend highly on the timing, there are also other factors such as cell passage number (Appendix A), quality of reagents, and many other variables that this model does not take into account. As such, if this method were to be used to quantify an unknown sample, it would have to be compared to a standard curve that was exposed to the same set of conditions. Consequently, a calibration curve should be made with a virus sample with known concentration to calculate the constants in the model for the specific set of conditions.

The strong correlation between the logarithm of the MOI and percent of cells with high granularity demonstrates a direct relationship prior to 24 hpi. From these studies, it can be shown that any time from 16 to 20 hpi will yield an accurate fit to the model in Equation 5. The sampling time point of 20 hpi will be used for further studies because it represents the time when there is a maximum granularity in the cells with an acceptable fit to the model.

Chapter 6

Validating Assay

6.1 Chapter Objective

The goal of this chapter is to demonstrate that the logarithmic model from Equation 5 can be used to predict the titer of unknown samples that will yield results comparable to a traditional plaque assay. The assay is translated into a 96-well format in order to achieve a higher throughput. Five samples of unknown titer donated by Sanofi were quantified using both the flow cytometric-based assay, which will be further referred to as the granularity-based flow assay, and plaque assay. The five samples differed by the length of time they were exposed to sonication. The granularity-based flow assay was conducted by creating a calibration curve to calculate the constants for the model and then this model was used to predict the infectious titer of the unknown samples.

6.2 Materials and Methods

6.2.1 Cell Maintenance

The complementary Vero cells (HSV2013-121) were maintained in Dulbecco's Modified Eagle Medium (DMEM) with F12 (Corning Cellgro, Manassas, VA) supplemented with 10% heat inactivated fetal bovine serum (FBS) (Gibco Life Technologies, Burlington, Canada), and 4mM L-glutamine (Sigma-Aldrich, Oakville, Canada) at 37^{o}C in 5% CO_2 in T-flasks. Viruses were stored at -80°C until infection. Virus sample A was exposed to 2 minutes of sonication, sample B was 4 minutes, sample C was 6 minutes, sample D was 8 minutes and sample E was produced by using a new extraction technique (undisclosed by Sanofi). All samples were titered using a plaque assay.

6.2.2 Infection of Cells Prior to Flow Cytometry

Complementary Vero cells were plated onto 96-well plates at a concentration of $3.0x10^4$ cells/well and incubated overnight. The next day, the spent media was aspirated and the cells were washed once with D-PBS. Virus samples were serially diluted (1:2 ratio) 8 times in ice cold cell maintenance media just prior to infection. The cells were subsequently incubated with 50 µL of diluted virus samples for 20 hpi.

6.2.3 Flow Cytometry Sample Preparation

After the specified infection time, the wells were aspirated and then the cells were treated with trypsin to detach cells from the surface of the plate. Once the cells were detached, an equal volume of 4% formaldehyde was added to the wells for a final volume of 200 µL and

then the sample was transferred in to 5 mL polystyrene culture tubes and stored at 4°C for 1 hour. After the cells were fixed, the samples were run through the FACScalibur to collect 2,000 events with the SSC photomultiplier tube (PMT) voltage set to 280 mV, the FL1 was set to 580 mV and, the FSC was set to E01 at the high flow setting (60 μL/min).

6.2.4 Data Analysis

The gating was conducted as previously described and a trend line was calculated using the data obtained from the 'Standard' virus sample. MATLAB's nlmfit function was used to calculate the constants for Equation 5 and the then MOIs of the unknown samples could be calculated based off the percent of the population with high granularity. The average was taken for all the serial dilutions to obtain the final titer and a variance between the dilutions.

6.3 Results

Samples with unknown viral titer were quantified using both the plaque assay and the new granularity-based flow assay to compare the two methods. A sample with known titer was used to produce a calibration curve (trend line in Figure 20) to correlate the percent of cells with high granularity with the concentration of virus. The constants calculated by the trend line were used to predict the viral titers for the unknown titers seen in Table 5. Each viral titer obtained from the granularity-based flow assay was calculated by taking the mean of the titer predicted from 7 viral dilutions (each dilution contains 3 replicates) for each sample. The data points in Figure 20 appear very close together at lower concentrations, and then vary farther from the trend line at the higher concentrations. This indicates that at very high MOI the results will have a larger variance.

The plaque assay used the average from three dilutions, and each dilution had triplicates. Although the granularity-based flow assay has a larger standard deviation (calculated from the variance of the dilutions) than the plaque assay, all the results are within the same magnitude with the highest percent difference being 52.67% (Table 5).

To determine the minimum levels of virus that are detectable using this new method, the lower limits of detection and quantification were calculated using the variation of the blank (n=47). The limit of detection (LOD) represents the lowest signal that can be reliably distinguished from the blank and can be detected[105]. It was calculated by taking the average of the blank ($\overline{x_b}$ =0.055) and then adding three times the standard deviation of the blank

($S_b = 0.0041$). The limit of quantification (LOQ) is the lowest concentration of virus that can be determined with acceptable precision and accuracy[106]. This was calculated by taking the average of the blank and then adding ten times the standard deviation of the blank. These two limits provided the granularity-based flow assay with the lower detection limits of 8,360 PFU/mL (MOI 0.01) for the LOD and 13,940 PFU/mL (MOI 0.02) for the LOQ (Figure 20). This indicates that this assay requires a concentration higher than 13,940 PFU/mL (MOI 0.02) in order to precisely and accurately predict the titer of sample.

A concordance plot was made to compare the viral titers predicted by using the plaque and granularity-based flow assays. At lower concentrations of virus, the granularity-based flow assay tends to underestimate the viral titer, but these values ($1.3x10^4$ PFU/mL) are around the limit of quantification. The range where there is the highest agreement, or where the results are relatively similar, between the two assays is between $6.0x10^4$ PFU/mL and $1x10^6$ (MOI of 2 to 33, respectively) (Figure 21). The correlation coefficient was calculated to be 0.70 with a p-value<0.001.

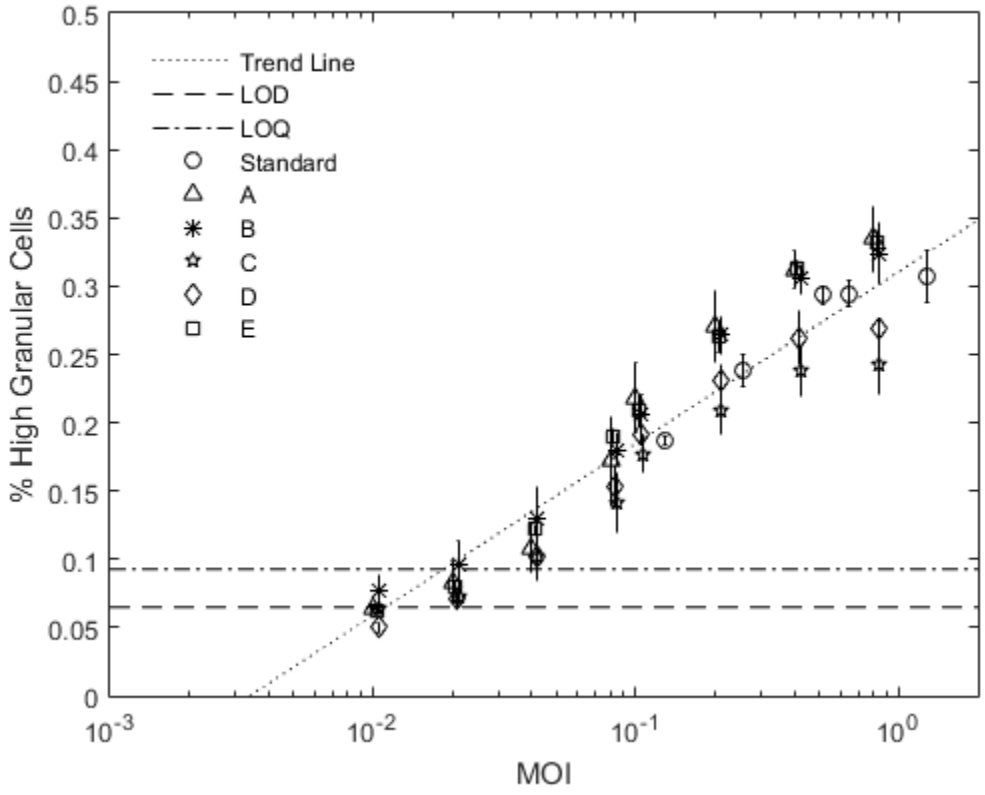

Figure 20- 5 samples with unknown titers quantified using plaque and granularity-based flow assay

A standard sample of known titer was used as a calibration curve to produce the trend line that relates the logarithm of the MOI to the percent of the sample population with highly granular cells with the following relationship:

$$\%\ \text{High Granular Cells} = 0.05464 \ln(\text{MOI}) + 0.3106$$

The unknown samples were diluted serially 7 times (in triplicate) and sampled after 20 hpi. Plaque assays were also conducted for samples A-E and their results are plotted here to demonstrate the deviation of the plaque assay results to the standard curve.

Table 5- Comparison of viral titer between plaque assay and granularity-based flow assay

The percent difference was calculated relative to the plaque assay.

Sample	Plaque Assay (10^6)	Coefficient of Variance	Granularity-based flow assay (10^6)	Coefficient of Variance	Difference between assays
A	6.00±0.691	11.52%	9.16±4.53	49.42%	-52.67%
B	6.33±2.05	32.41%	8.94±3.00	33.52%	-41.32%
C	6.34±0.586	9.24%	4.13±1.33	32.17%	34.85%
D	6.28±0.827	13.17%	4.96±1.50	30.23%	21.01%
E	61.7±11.3	18.32%	90.3±39.1	43.26%	-46.45%

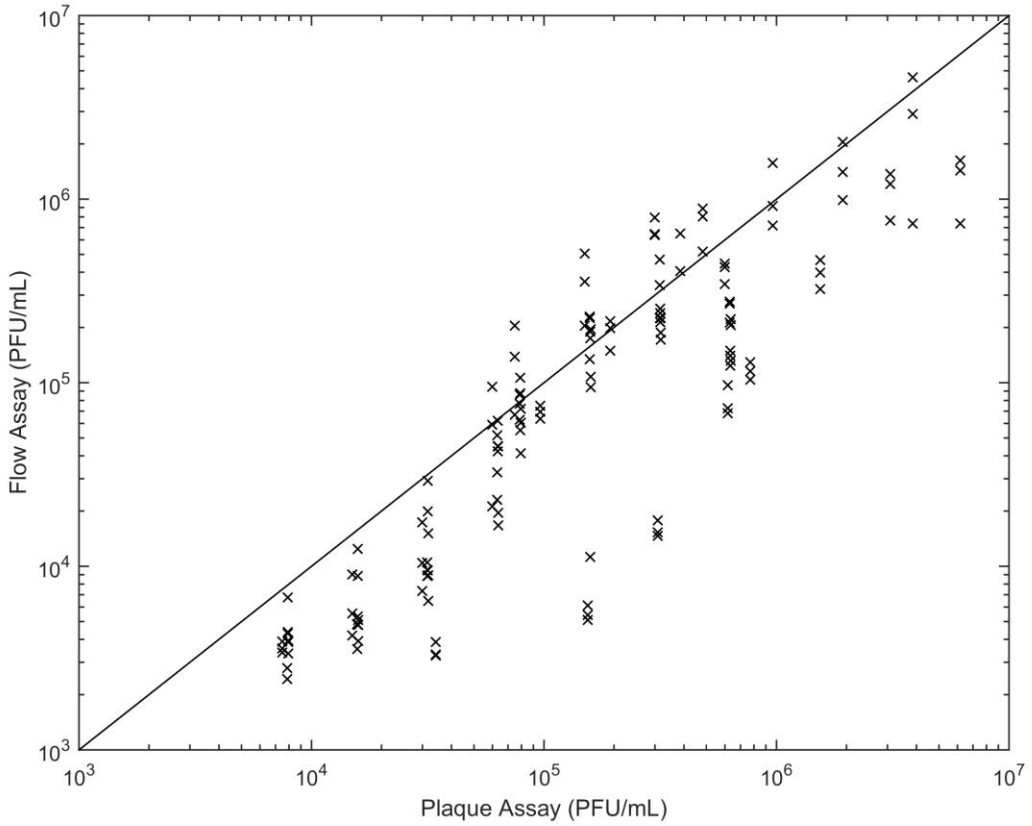

Figure 21- Concordance plot comparing the granularity-based flow assay and plaque assay

The data points from 6 different samples with 7 separate dilutions are plotted demonstrating the concordance between the natural logarithm of the plaque assay results to those of the granularity-based flow assay. The solid line is the line representing perfect concordance and the 'x' are the individual data points.

6.4 Discussion

The assay developed here uses the natural increase in granularity in infected complementary non-GFP Vero cells by ACAM529 to predict the infectious titer. In order to evaluate the accuracy of this method, 5 unknown samples were titered using the granularity-based flow assay and the plaque assay. For the granularity-based flow assay, a calibration curve had to be created using a standard viral sample with known titer. From this calibration curve the amount of granular cells could be correlated to an infectious viral titer. It was found that the granularity-based flow assay was able to obtain similar results as the plaque assay. The accuracy was evaluated by calculating the percent difference between the two samples which had a maximum difference of -52.67%, indicating a suitable closeness to the true value. The coefficient of variance (CV) was also calculated to demonstrate the dispersion of data for both assays. The plaque assay has a lower variance than the granularity-based flow assay. This indicates that the granularity-based flow assay is less precise than the plaque assay. Precise measurements are not necessarily accurate, since precision refers to the relative agreement of the samples, while accuracy is used to describe the closeness to the true value. It is possible that due to operator bias, the results from a plaque assay can be precise, but not necessarily accurate.

The titers calculated from the plaque assay are within one standard deviation of the granularity-based flow assay, so a 95% confidence interval of the granularity-based flow assay would contain the correct titer but there would be a greater amount of uncertainty associated with the result.

Due to the requirement of having greater than 13,940 PFU/mL (MOI 0.02) in solution due to the LOQ, this assay will only be relevant in applications that require the enumeration of virus stocks of high concentration, such as in the manufacturing of viruses in the biopharmaceutical industry. The benefit of this assay is that it can be translated into a high throughput method that takes a maximum of 20 hours incubation time, and also reduces the potential for operator bias which is present in plaque assays. While it does offer the advantage of speed, the higher cost of the equipment and need for specialized training are two major drawbacks to this new method.

Chapter 7

Infection of QT-35 Cells with ALVAC.gfp

7.1 Chapter Objective

The aim of this chapter is to illustrate that the flow cytometric-based assay could be used for other cell-virus systems. Here, we used QT-35 cells infected with ALVAC.gfp virus which contains the GFP gene. Once the cells became infected they began to produce GFP, which is an indicator of successful infection of the cell. The cells which produce GFP are positive indicators of infection, and the change in granularity of the cells was investigated. A time course was conducted to observe the optimal time point to measure the level of granularity. Then at the optimal time point, a range of MOIs were tested to investigate if Equation 5 was still a valid model to correlate infectious titer to the percent of the population with high granularity.

7.2 Materials and Methods

7.2.1 Cell Line and Virus

The ALVAC.gfp virus was stored at -80ºC and thawed in a 37ºC water bath immediately before use. The QT-35 cells were maintained as previously stated in Chapter 3.

7.2.2 Flow Cytometry Sample Preparation

Cells were plated on a 96-well plate at a concentration of $3.0x10^4$ cells per well and incubated overnight. The infection was complete as previously stated. After the specified infection time, the wells were aspirated and then the cells were treated with trypsin to detach cells from the surface of the plate. Once the cells were detached, an equal volume of 4% formaldehyde was added to the wells and the sample was transferred into 5 mL polystyrene culture tubes and stored at 4°C for 1 hour. The final volume for a 96-well plate was 200 μL. After the cells were fixed, the samples were run through the FACScalibur to collect 2,000 events with the SSC photomultiplier tube (PMT) voltage set to 280 mV, the FL1 was set to 580 mV and, the FSC was set to E00 at the high flow setting (60 μL/min).

7.2.3 Data Analysis

Data was analyzed as previously stated.

7.2.4 Cell Culture Infectious Dose 50 ($CCID_{50}$)

QT-35 cells were plated into a 96-well plate at a concentration of $3x10^4$ cells per well and infected with serially diluted ALVAC.gfp virus with 10 replicates. After 5-8 days, the plate was scored for cytopathic effect and the titer was calculated. To score the cytopathic effect, each well was visually inspected for signs of infection in the cells. The wells are score Yes/No for infection and then the 50% infectious dose can be calculated using the formula for the end point dilution assay as reviewed on page 29.

7.2.5 Immunostaining

To confirm infection, $6.0x10^5$ cells were grown on 6-well plates overnight, washed once with D-PBS and infected. After 24 hpi, the media was aspirated and the cells were treated with trypsin for 10 minutes. The infected cells and uninfected control were stained for 30 minutes at room temperature with 100µL of CytoPainter (Abcam, Cambridge, MA; used at a 1:1000 dilution) washed two times using D-PBS. Samples were then transferred into 1.5 mL microcentrifuge tubes for flow cytometric measurements and imaging using ImageStream^X.

CytoPainter is used to stain actin filaments in the cell. By staining the cytoskeleton of the cell we can obtain a better idea of the structure of the cell.

7.3 Results

QT-35 cells were infected with ALVAC.gfp virus to assess the change in granularity of the cells 24 hours post infection. Upon successful infection, cells began to produce GFP which could be monitored using a flow cytometer (Figure 23A&B). The maximum levels of GFP production could be seen at 24-28 hours after infection (Figure 22). The levels of intensity of the green fluorescence produced by the QT-35 cells after 24 hours was assessed for uninfected and infected cells (MOI 3) using an imaging flow cytometer and used as an indicator of successful infection in the cells (Figure 23). A histogram of the side scatter values of the infected and uninfected populations demonstrates that there is significant increase in the number of cells with high granularity (Figure 23D).

To assess whether the increase in the number of cells with high granularity can be correlated to the initial MOI, serial dilutions of ALVAC.gfp were used to infect QT-35 and incubated for 24 hours. The percent of the sample population with high levels of side scatter was plotted versus the MOI, calculated by a $CCID_{50}$ assay. A direct correlation between the two variables was observed beyond MOI 4.6 (Figure 24). To obtain a range of accurate measurement for this assay the LOD and LOQ were calculated based on the variability of the blank (n=94). It was found that the limit of detection was 450 PFU/mL and the limit of quantification was 990 PFU/mL (or in terms of MOI 0.14 and 4.6 respectively).

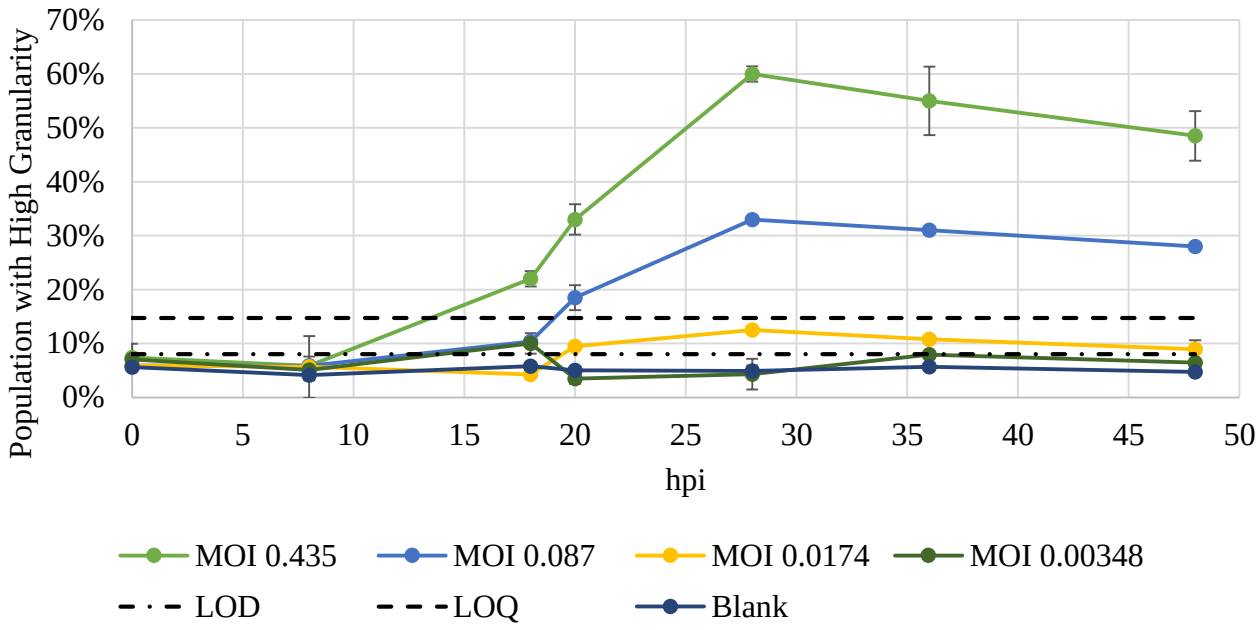

Figure 22- Tracking the increase in the fraction of the population of QT-35 cells infected with ALVAC.gfp with increased granularity over 48 hours

Error bars are the standard deviation obtained from triplicates.

A.

B.

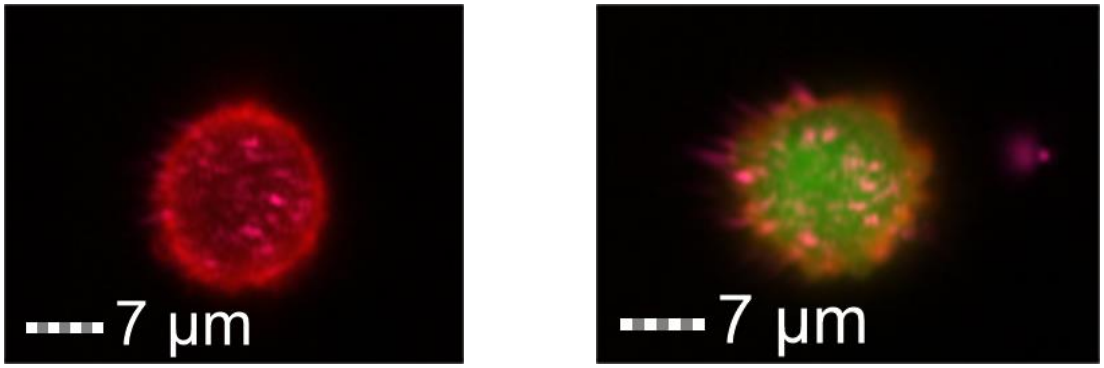

C.

D.

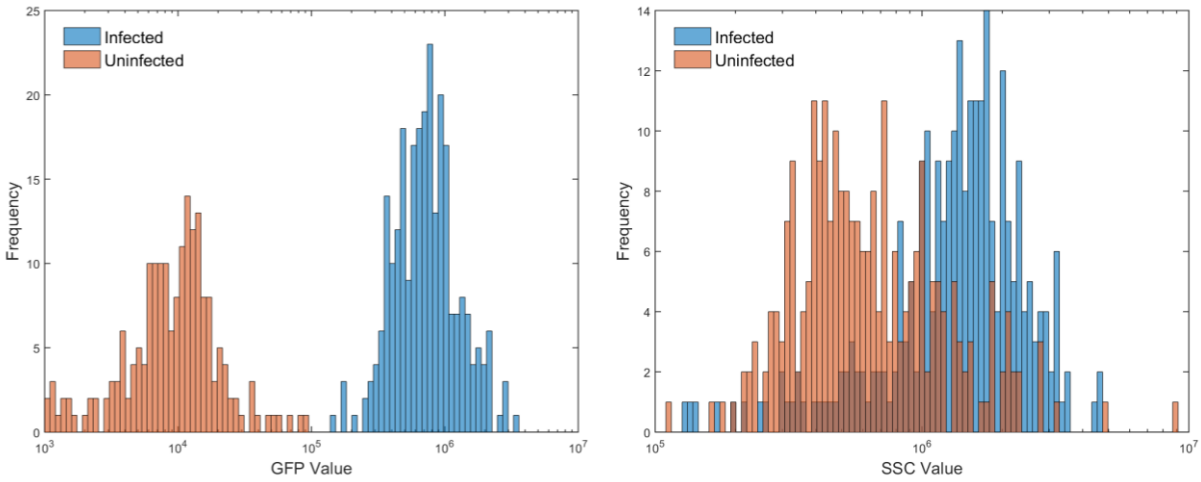

Figure 23- Confirmation by GFP production that infected QT-35 cells have increased granularity 24 hpi

QT-35 cells were infected at a MOI of 3 and incubated with the virus for 24 hours. A. An uninfected cell stained with CytoPainter shows no GFP production. B. An infected cell stained with Cytopainter has relatively the same size as an uninfected cell, but is producing GFP after infection with ALVAC.gfp. C. A histogram of the green fluorescence where the infected (blue) and uninfected (pink) are shown. There is a distinct difference in the levels of GFP in the two populations. D. The uninfected (pink) and infected (blue) regions are shown on a side scatter histogram. Here the two regions overlap, but a bimodal curve can still be seen. The median of the infected ($1.42x10^6$ IU) and uninfected ($5.68x10^5$ IU) samples are significantly different ($\alpha=0.001$, $p<0.001$), as calculated by the Wilcoxon rank sum test.

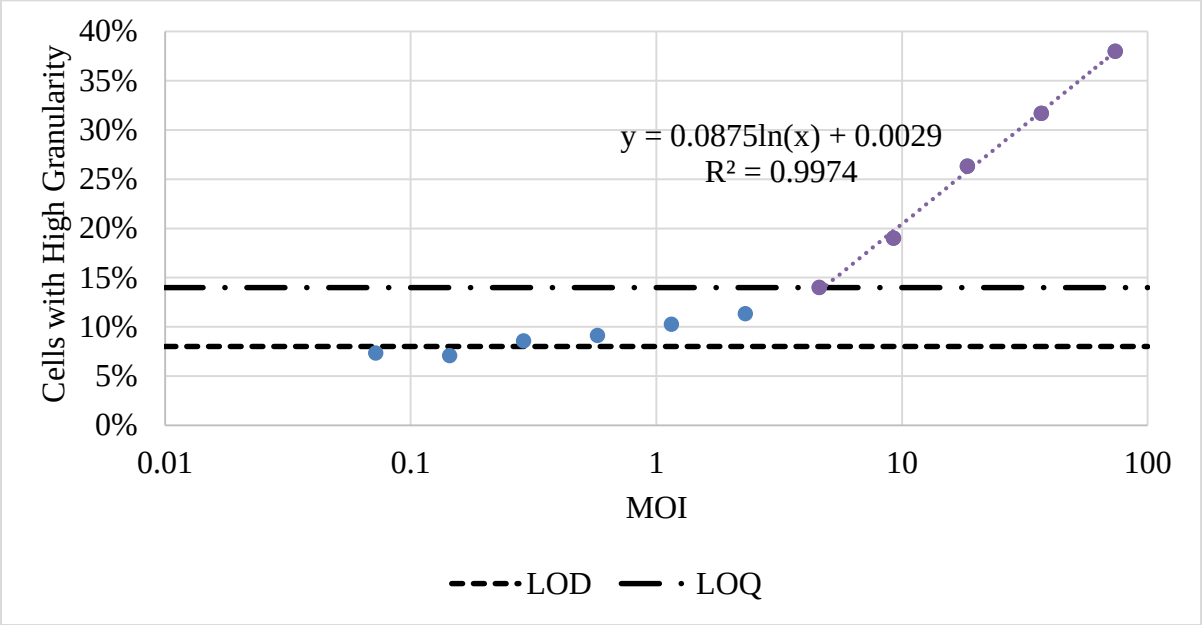

Figure 24-The percent of QT-35 cells displaying high granularity after 24 hpi fit to same model as ACAM529 infection in complementary non-GFP Vero cells

A sample of ALVAC.gfp was diluted 7 times in triplicate to demonstrate a logarithmic relationship between the MOI and percent of the population with high granularity. The blue data points represent the data from the experiment that is below the limit of quantification, and this data is not included in the trend line. The purple data points represent the data that is above the limit of quantification and were used to make the trend line (dashed purple line).

7.4 Discussion

An increase in granularity in QT-35 cells after infection was positively correlated with time and MOI. The increase in granularity of an infected population was significantly different than that of an uninfected population, demonstrating the principle that was seen with the ACAM529 virus in the complementary non-GFP Vero cell line. The increase in the granularity of the infected cells was most likely caused by inclusion bodies that canarypox forms during viral replication. These inclusion bodies are produced in the cytoplasm and are believed to function as viral replication sites where the necessary components for replication are concentrated to hasten viral assembly and maturation[83]. Although, it is equally likely that the increase in granularity could be attributed to the increase of the total amount of viral proteins in the cell causing an increase in the intracellular complexity. The maximum amount of cells in the population which displayed high levels of granularity occurred at approximately 28 hpi, which is earlier than what was seen for ACAM529. The replication cycle for canarypox is estimated to be 3-5 days which is much longer than that of the herpes simplex virus which takes approximately 20-24 hours. Therefore, it seems unlikely that the true maximum occurs at 28 hpi, but rather this is a plateau, such as the one seen from 16-20 hpi with ACAM529. This plateau could suggest that the virus has finished one phase of its replication such as producing viral components, or the formation of the inclusion bodies, before it begins the next steps.

Nevertheless, the goal of the granularity-based flow assay is to decrease the time required to quantify the infectious titer of the virus, which is accomplished here. The time required to obtain a titer using the $CCID_{50}$ is 5-8 days, and the time for the granularity-based flow assay

is 24 hours. As previously noted with the ACAM529/Vero cell system, the granularity-based flow assay is limited since it requires a high concentration of virus due to the LOQ (990 PFU/mL or MOI 4.6). This limit of quantification is less than the one calculated for ACAM529, which indicates that the sensitivity of the assay is dependent on the particular cell/virus system.

Chapter 8

Conclusions

8.1 Herpes/Vero System

Three parameters (green fluorescence, granularity and forward scatter) were tested to determine a relationship between a parameter and infectious titer of the virus. It was found that the complementary GFP Vero cell line which contains GFP encoding genes, produced a large amount of basal level of GFP such that green fluorescence was not an optimal parameter to use to measure infectivity of the virus. For forward scattered light, the mean of the histogram for the population of infected cells did not change over time. Alternatively, the median for the side scattered light did increase over time. The increase in side scattered light (i.e. granularity) was also seen in complementary non-GFP Vero cells. Changes in granularity of the cells were not found to be caused by cytokine or other cell signalling molecules in the virus sample, and the increase in granularity was found to be dependent on viral replication. It was also confirmed that it was indeed infected cells that had a higher average level of granularity (through the use of immunostaining).

To determine the optimal time point to measure the granularity of infected cells, a 72 hour time course was done to track the levels of granularity of cells using 5 different MOIs. An incubation of 16 and 20 hpi resulted in the best relationship between the number of cells with increased granularity and MOI. At these times a logarithmic model relating the percent of the population with elevated levels of granularity and the infectious titer of the virus. It was also

seen, however, that the assay was time sensitive and therefore much care needed to be taken to rapidly infect the cells so that the assumption of a uniform incubation held.

Five unknown samples were titered using both the granularity-based flow assay and the plaque assay. It was found that the granularity-based flow assay had a larger variance than the plaque assay, but obtained accurate results. The coefficient of concordance was found to be 0.7, which demonstrates that the granularity-based flow assay had the tendency to underestimate the infectious titer of the virus. This assay also required that there was at least 13,940 PFU/mL (MOI 0.02) due to the limit of quantification. This restricts the use of this new assay to applications that produce high concentrations of virus, which does not make it ideal for clinical applications which requires the assay to be sensitive enough to detect a single infectious virion. This is appropriate for process analysis for the biopharmaceutical industry where a high concentration is desired and diluting the virus stock is an additional step which could increase the error in the quantification process.

While the granularity-based flow assay had a greater amount of variance and requires high concentrations of virus, this new assay reduced the time by a maximum of 32 hours and has been developed for a 96-well format. This allows users to quantify several samples of virus at once and will decrease the time necessary to calculate the efficiency of a production process.

8.2 ALVAC/QT-35 System

A second cell line and virus were used to test the extension of the assay with other systems. An increase in granularity was also seen in QT-35 cells infected with ALVAC.gfp, with positive correlations with time and MOI. It was confirmed that the population that displayed

green fluorescence (proof of infection) also had an elevated level of granularity. The percent of the population that displayed an increased amount of granularity was correlated to MOI using a logarithmic relationship similar to that of the Vero/ACAM529 system. Together, these findings suggest that the ALVAC.gfp virus can be titered using the granularity-based flow assay. By using this new assay, the time required to obtain an infectious titer would decrease from 5-8 days to 24 hours. As previously stated, this will aid in process improvement by decreasing the time it takes to quantify the efficiency of each production step.

Chapter 9

Recommendations

The assay that is proposed in this thesis demonstrates the possibility of using naturally occurring changes in the cell to identify infection. It has shown that through the use of flow cytometry, the physiological changes in cells post-infection can be modelled using a logarithmic relationship to relate the percent of the population with high granularity to MOI. It also gave evidence that these changes occur in multiple cell lines after infection. Although, the increase in granularity has been noted by previous authors in HEK293[20] and Sf9[19,21] cells lines, none have investigated the reason for the change. As such, there are still questions to be answered, such as the root cause of the increase in granularity and why the maximum amount of cells displaying high granularity only reaches 57% and not 100% for very high MOIs. Therefore, in order to complete the story of this assay, these subjects should be investigated to elucidate the true cause for the increase in granularity of cells post-infection.

In order to improve upon the logarithmic model used in this thesis, incubation time should be included as one of the parameters. From the data, it was seen that the difference of two hours produced a very large change in the amount of granularity seen in the cells from 16 to 20 hours. A new logistic model should be used to include the effect of time along with MOI to model the percent of the population with high granularity. By including the variable of time in the model, there will no longer be a need to make the assumption of instantaneous infection of the 96-well plate. Also, to ensure that there is synchronous infection, after 1 hpi,

the cells should be washed with D-PBS to remove any unattached virions. This will remove some of the variability associated with virus infection time.

Furthermore, to provide more evidence for the reliability of this method, more concordance studies should be done using multiple operators and flow cytometers to demonstrate that the correlation between infectious titer and amount of cells displaying high granularity is not an artifact of a single operator and flow cytometer. Concordance studies with multiple operators will allow the operator-to-operator variability to be determined, which is a known disadvantage of the plaque assay.

The work presented in this thesis provides a first step in developing an enumeration technique that uses the change in granularity of cells to estimate the viral titer. The recommendations stemming from this work focus on elucidating the causes for the increase in granularity and further improving the model that estimates viral titer as well as the variances associated with this model.

References

1. Services, H. Guidance for Industry Q5A Viral Safety Evaluation Derived From Cell Lines of Human or Animal Origin Guidance for Industry. (1998).

2. *U.S. Vaccines*. *Epidemiology and Prevention of Vaccine-Preventable Diseases* **1,** (2015).

3. Wirth, T., Parker, N. & Ylä-Herttuala, S. History of gene therapy. *Gene* **525,** 162–169 (2013).

4. Tartaglia, J. *et al.* Therapeutic vaccines against melanoma and colorectal cancer. *Vaccine* **19,** 2571–2575 (2001).

5. Sheridan, C. Amgen announces oncolytic virus shrinks tumors. *Nat. Biotechnol.* **31,** 471–472 (2013).

6. Palomares, L. A., Realpe, M. & Ramírez, O. T. in *Journal of Clinical Pathology* **43,** 501–519 (2015).

7. Mettenleiter, T. C. Mini Review: Herpesvirus Assembly and Egress. *J. Virol.* **76,** 1537–1547 (2002).

8. Virocyt, I. White Paper : an Overview of Virus Quantification Techniques. 1–5 (2013).

9. Azizi, A., Tang, M., Gisonni-Lex, L. & Mallet, L. Evaluation of infectious titer in a candidate HSV type 2 vaccine by a quantitative molecular approach. *BMC Microbiol.* **13,** 284 (2013).

10. Morgan, M. a & Smith, T. F. Evaluation of an enzyme-linked immunosorbent assay for the detection of herpes simplex virus antigen. *J. Clin. Microbiol.* **19,** 730–732 (1984).

11. LaBarre, D. D. & Lowy, R. J. Improvements in methods for calculating virus titer estimates from TCID50 and plaque assays. *J. Virol. Methods* **96,** 107–126 (2001).

12. Li, Z., Ling, L., Liu, X., Laus, R. & Delcayre, A. A flow cytometry-based immuno-titration assay for rapid and accurate titer determination of modified vaccinia Ankara virus vectors. *J. Virol. Methods* **169,** 87–94 (2010).

13. Grigorov, B., Rabilloud, J., Lawrence, P. & Gerlier, D. Rapid titration of measles and other viruses: optimization with determination of replication cycle length. *PLoS One* **6,** e24135 (2011).

14. Lonsdale, R. *et al.* A rapid method for immunotitration of influenza viruses using flow cytometry. *J. Virol. Methods* **110,** 67–71 (2003).

15. McSharry, J. J. Analysis of virus-infected cells by flow cytometry. *Methods* **21,** 249–57 (2000).

16. Foster, T. P., Rybachuk, G. V & Kousoulas, K. G. Expression of the enhanced green fluorescent protein by herpes simplex virus type 1 (HSV-1) as an in vitro or in vivo marker for virus entry and replication. *J. Virol. Methods* **75,** 151–60 (1998).

17. Kung, S. H., Wang, Y. C., Lin, C. H., Kuo, R. L. & Liu, W. T. Rapid diagnosis and quantification of herpes simplex virus with a green fluorescent protein reporter system. *J. Virol. Methods* **90,** 205–12 (2000).

18. Gervaix, A. *et al.* A new reporter cell line to monitor HIV infection and drug susceptibility in vitro. *Proc. Natl. Acad. Sci. U. S. A.* **94,** 4653–8 (1997).

19. Nordström, T., Willamo, P., Arvela, M., Stenroos, K. & Lindqvist, C. Detection of baculovirus-infected insect cells by flow cytometric side-scatter analyses. *Cytometry* **37,** 238–42 (1999).

20. Sandhu, K. S. & Al-Rubeai, M. Monitoring of the adenovirus production process by flow cytometry. *Biotechnol. Prog.* **24,** 250–61 (2008).

21. Qi, J., Liu, T., Pan, J., Miao, P. & Zhang, C. Rapid baculovirus titration assay based on viable cell side scatter (SSC). *Anal. Chim. Acta* 3–7 (2015). doi:10.1016/j.aca.2015.04.007

22. Xu, F. *et al.* Trends in herpes simplex virus type 1 and type 2 seroprevalence in the United States. *Jama* **296,** 964–73 (2006).

23. Tronstein, E. *et al.* Genital shedding of Herpes Simplex Virus among symptomatic and asymptomatic persons with HSV-2 infection. **305,** 1441–1449 (2014).

24. Holmberg, S. D. *et al.* Prior Herpes Simplex Virus Type 2 infection as a risk factor for HIV infection. (2014).

25. Corey, L., Wald, A., Celum, C. L. & Quinn, T. C. The effects of Herpes Simplex Virus-2 on HIV-1 acquisition and transmission: A review of two overlapping epidemics. *JAIDS J. Acquir. Immune Defic. Syndr.* **35,** 435–445 (2004).

26. Awasthi, S. *et al.* Immunization with a vaccine combining herpes simplex virus 2 (HSV-2) glycoprotein C (gC) and gD subunits improves the protection of dorsal root ganglia in mice and reduces the frequency of recurrent vaginal shedding of HSV-2 DNA in guinea pigs compared to. *J. Virol.* **85,** 10472–86 (2011).

27. Cattamanchi, A. *et al.* Phase I study of a herpes simplex virus type 2 (HSV-2) DNA vaccine administered to healthy, HSV-2-seronegative adults by a needle-free injection system. *Clin. Vaccine Immunol.* **15,** 1638–43 (2008).

28. Görander, S., Harandi, A. M., Lindqvist, M., Bergström, T. & Liljeqvist, J.-Å. Glycoprotein G of herpes simplex virus 2 as a novel vaccine antigen for immunity to genital and neurological disease. *J. Virol.* **86,** 7544–53 (2012).

29. Morello, C. S. *et al.* Inactivated HSV-2 in MPL/alum adjuvant provides nearly complete protection against genital infection and shedding following long term challenge and rechallenge. *Vaccine* **30,** 6541–50 (2012).

30. Dolan, A., Jamieson, F. E., Cunningham, C., Barnett, B. C. & Geoch, D. J. M. C. The genome sequence of Herpes Simplex Virus Type 2. *J. Virol.* **72,** 2010–2021 (2010).

31. Segura, M. M., Kamen, A. A. & Garnier, A. Viral Vectors for Gene Therapy. **737,** (2011).

32. Whitley, R. J. & Roizman, B. Herpes simplex virus infections. *Lancet* **357,** 1513–8 (2001).

33. Panagiotidis, C., Lium, E. & Silverstein, S. Physical and functional interactions between herpes simplex virus immediate-early proteins ICP4 and ICP27. *J. Virol.* **71,** 1547–1557 (1997).

34. Mettenleiter, T. C., Klupp, B. G. & Granzow, H. Herpesvirus assembly: a tale of two membranes. *Curr. Opin. Microbiol.* **9,** 423–9 (2006).

35. Mettenleiter, T. C., Klupp, B. G. & Granzow, H. Herpesvirus assembly: an update. *Virus Res.* **143,** 222–34 (2009).

36. Brown, J. & Newcomb, W. Herpesvirus capsid assembly: insights from structural analysis. *Curr. Opin. Virol.* **1,** 142–149 (2011).

37. Roizman, B., Knipe, D. M. & Whitley, R. J. in *Fields Virology* 1824–1893 (LWW, 2013). doi:616.9/101

38. Johnson, D. C. & Baines, J. D. Herpesviruses remodel host membranes for virus egress. *Nat. Rev. Microbiol.* **9,** 382–94 (2011).

39. Taddeo, B., Zhang, W. & Roizman, B. The herpes simplex virus host shutoff RNase degrades cellular and viral mRNAs made before infection but not viral mRNA made after infection. *J. Virol.* **87,** 4516–22 (2013).

40. Milligan, G. N., Dudley-McClain, K. L., Young, C. G. & Chu, C.-F. T-cell-mediated mechanisms involved in resolution of genital herpes simplex virus type 2 (HSV-2) infection of mice. *J. Reprod. Immunol.* **61,** 115–27 (2004).

41. Spear, P. & Longnecker, R. Herpesvirus entry: an update. *J. Virol.* **77,** 10179–10185 (2003).

42. Spear, P. G. Herpes simplex virus: receptors and ligands for cell entry. *Cell. Microbiol.* **6,** 401–10 (2004).

43. Akhtar, J. & Shukla, D. Viral entry mechanisms: cellular and viral mediators of herpes simplex virus entry. *FEBS J.* **276,** 7228–7236 (2009).

44. Herold, B. C., Visalli, R. J., Susmarski, N., Brandt, C. R. & Spear, P. G. Glycoprotein C-independent binding of herpes simplex virus to cells requires cell surface heparan sulphate and glycoprotein B. *J. Gen. Virol.* **75,** 1211–1222 (1994).

45. Herold, B. C., Wudunn, D., Soltys, N. & Spear, P. G. Glycoprotein C of Herpes Simplex Virus Type 1 plays a principal role in the adsorption of virus to cells and in infectivity. *J. Virol.* **65,** 1090–1098 (1991).

46. Zaichick, S. V, Bohannon, K. P. & Smith, G. a. Alphaherpesviruses and the cytoskeleton in neuronal infections. *Viruses* **3,** 941–81 (2011).

47. Oh, M., Akhtar, J., Desai, P. & Shukla, D. A role for heparan sulfate in viral surfing. *Biochem. Biophys. Res. Commun.* **391,** 176–181 (2010).

48. Clement, C. *et al.* A novel role for phagocytosis-like uptake in herpes simplex virus entry. *J. Cell Biol.* **174,** 1009–21 (2006).

49. Kukhanova, M. K., Korovina, a. N. & Kochetkov, S. N. Human herpes simplex virus: Life cycle and development of inhibitors. *Biochem.* **79,** 1635–1652 (2015).

50. Weller, S. K. & Coen, D. M. Herpes Simplex Viruses: Mechanisms of DNA Replication. *Cold Spring Harb. Perspect. Biol.* **4,** a013011–a013011 (2012).

51. Weller, S. K. Herpes simplex virus reorganizes the cellular DNA repair and protein quality control machinery. *PLoS Pathog.* **6,** 1–3 (2010).

52. Sandri-Goldin, R. M. Replication of the herpes simplex virus genome: does it really go around in circles? *Proc. Natl. Acad. Sci. U. S. A.* **100,** 7428–7429 (2003).

53. Wild, P. *et al.* Exploring the nuclear envelope of herpes simplex virus 1-infected cells by high-resolution microscopy. *J. Virol.* **83,** 408–419 (2009).

54. Mettenleiter, T. Herpesvirus assembly and egress. *J. Virol.* **76,** 1537–1547 (2002).

55. Stackpole, C. W. Herpes-type virus of the frog renal adenocarcinoma I. Virus development in tumor transplants maintained at low temperature. *J. Virol.* **4,** 75–93 (1969).

56. Wild, P. *et al.* Impairment of nuclear pores in bovine herpesvirus 1-infected MDBK cells. *J. Virol.* **79,** 1071–1083 (2005).

57. Johnson, D. C. & Spear, P. G. Monensin inhibits the processing of herpes simplex virus glycoproteins, their transport to the cell surface, and the egress of virions from infected cells. *J. Virol.* **43,** 1102–1112 (1982).

58. Campadelli-Fiume, G. in *Human Herpesviruses: Biology, Therapy, and Immunoprophylaxis* (eds. Arvin, A. et al.) (Cambridge University Press, 2007).

59. Dingwell, K. S. *et al.* Herpes simplex virus glycoproteins E and I facilitate cell-to-cell spread in vivo and across junctions of cultured cells. *J. Virol.* **68,** 834–45 (1994).

60. Farnsworth, A. & Johnson, D. C. Herpes Simplex Virus gE/gI must accumulate in the trans - Golgi Network at early times and then redistribute to cell junctions to promote cell-cell spread. *J. Virol.* **80,** 3167–3179 (2006).

61. Johnson, D. C., Webb, M., Wisner, T. W. & Brunetti, C. Herpes simplex virus gE/gI sorts nascent virions to epithelial cell junctions, promoting virus spread. *J. Virol.* **75,** 821–33 (2001).

62. Salameh, S., Sheth, U. & Shukla, D. Early Events in Herpes Simplex Virus Lifecycle with Implications for an Infection of Lifetime. *Open Virol. J.* **6,** 1–6 (2012).

63. Grandi, G. & Nagy, E. *Development of novel vaccines*. (Springer-Verlag Wien, 2012). doi:10.1007/978-3-7091-0709-6

64. Zanotto, C. *et al.* Canarypox and fowlpox viruses as recombinant vaccine vectors: A biological and immunological comparison. *Antiviral Res.* **88,** 53–63 (2010).

65. Weli, S. C. & Tryland, M. Avipoxviruses: infection biology and their use as vaccine vectors. *Virol. J.* **8,** 49 (2011).

66. Imoukhuede, E. B. *et al.* Safety and immunogenicity of the malaria candidate vaccines FP9 CS and MVA CS in adult Gambian men. *Vaccine* **24,** 6526–6533 (2006).

67. Kaufman, H. L. *et al.* Combination chemotherapy and ALVAC-CEA/B7.1 vaccine in patients with metastatic colorectal cancer. *Clin. Cancer Res.* **14,** 4843–4849 (2008).

68. Pialoux, G. *et al.* Lipopeptides induce cell-mediated anti-HIV immune responses in seronegative volunteers. *AIDS* **15,** 1239–1249 (2001).

69. Rerks-Ngarm, S. *et al.* Vaccination with ALVAC and AIDSVAX to prevent HIV-1 infection in Thailand. *N. Engl. J. Med.* **361,** 2209–2220 (2009).

70. Carithers, D. *Biological and immunogenic properties of Canarypox vectored vaccines*. (1995).

71. Taylor, J. *et al.* Biological and immunogenic properties of a canarypox-rabies recombinant, ALVAC-RG (vCP65) in non-avian species. *Vaccine* **13,** 539–549 (1995).

72. Pardo, M. C., Bauman, J. E. & Mackowiak, M. Protection of dogs against canine distemper by vaccination with a canarypox virus recombinant expressing canine distemper virus fusion and hemagglutinin glycoproteins. *Am. J. Vet. Res.* **58,** 833–836 (1997).

73. Siger, L. *et al.* Assessment of the efficacy of a single dose of a recombinant vaccine against West Nile virus in response to natural challenge with West Nile virus-infected mosquitoes in horses. *Am. J. Vet. Res.* **65,** 1459–1462 (2004).

74. Minke, J. M. *et al.* Recombinant canarypoxvirus vaccine carrying the prM/E genes of West Nile virus protects horses against a West Nile virus-mosquito challenge. *Arch. Virol. Suppl.* 221–230 (2004).

75. Poulet, H. *et al. Efficacy of a canarypox virus-vectored vaccine against feline leukaemia. The Veterinary record* **153,** (2003).

76. Hofmann-Lehmann, R. *et al.* Reassessment of feline leukaemia virus (FeLV) vaccines with novel sensitive molecular assays. *Vaccine* **24,** 1087–1094 (2006).

77. Minke, J. M., Audonnet, J. C. & Fischer, L. Equine viral vaccines: The past, present and future. *Veterinary Research* **35,** 425–443 (2004).

78. Pancholi, P. *et al.* DNA prime/canarypox boost-based immunotherapy of chronic hepatitis B virus infection in a chimpanzee. *Hepatology* **33,** 448–454 (2001).

79. Pancholi, P. *et al.* DNA prime-canarypox boost with polycistronic hepatitis C virus (HCV) genes generates potent immune responses to HCV structural and nonstructural proteins. *J. Infect. Dis.* **182,** 18–27 (2000).

80. *ICTVdB - The Universal Virus Database: Avipoxvirus*. (2006). at <http://ictvdb.bio-mirror.cn/ICTVdB/00.058.1.03.htm>

81. Tulman, E. R. *et al.* The genome of canarypox virus. *J. Virol.* **78,** 353–366 (2004).

82. SIB Swiss Institute of Bioinformatics. Avipoxvirus. (2014). at <http://viralzone.expasy.org/all_by_protein/151.html#tab7>

83. Sadasiv, E. C., Chang, P. W. & Gulka, G. Morphogenesis of canary poxvirus and its entrance into inclusion bodies. *Am. J. Vet. Res.* **46,** 529–535 (1985).

84. Aucoin, M. G., Perrier, M. & Kamen, A. a. Critical assessment of current adeno-associated viral vector production and quantification methods. *Biotechnol. Adv.* **26,** 73–88 (2008).

85. Legoff, J. *et al.* Real-time PCR quantification of genital shedding of herpes simplex virus (HSV) and human immunodeficiency virus (HIV) in women coinfected with HSV and HIV. *J. Clin. Microbiol.* **44,** 423–432 (2006).

86. Aryee, E. a N., Bailey, R. L., Natividad-Sancho, A., Kaye, S. & Holland, M. J. Detection, quantification and genotyping of Herpes Simplex Virus in cervicovaginal secretions by real-time PCR: a cross sectional survey. *Virol. J.* **2,** 61 (2005).

87. Reed, L. J. & Muench, H. A simple method of estimating fifty per cent endpoints. *Am. J. Hyg.* **27,** 493–497 (1938).

88. Daelemans, D., Pauwels, R., De Clercq, E. & Pannecouque, C. A time-of-drug addition approach to target identification of antiviral compounds. *Nat. Protoc.* **6,** 925–933 (2011).

89. Bernard, M.-C. *et al.* Immunogenicity, Protective Efficacy, and Non-Replicative Status of the HSV-2 Vaccine Candidate HSV529 in Mice and Guinea Pigs. *PLoS One* **10,** e0121518 (2015).

90. Hoshino, Y. *et al.* Protection from herpes simplex virus (HSV)-2 infection with replication-defective HSV-2 or glycoprotein D2 vaccines in HSV-1-seropositive and HSV-1-seronegative guinea pigs. *J. Infect. Dis.* **200,** 1088–95 (2009).

91. Domínguez, J., Lorenzo, M. M. & Blasco, R. Green fluorescent protein expressed by a recombinant vaccinia virus permits early detection of infected cells by flow cytometry. *J. Immunol. Methods* **220,** 115–21 (1998).

92. Gates, I. V *et al.* Quantitative measurement of varicella-zoster virus infection by semiautomated flow cytometry. *Appl. Environ. Microbiol.* **75,** 2027–36 (2009).

93. Vengatesan, D., Raj, G. D., Raja, A., Ramadass, P. & Gunaseelan, L. Detection of rabies virus antigen or antibody using flow cytometry. *Cytometry B. Clin. Cytom.* **70,** 335–43 (2006).

94. Soboleski, M. R., Oaks, J. & Halford, W. P. Green fluorescent protein is a quantitative reporter of gene expression in individual eukaryotic cells. *FASEB J.* **19,** 440–2 (2005).

95. Pollara, G. *et al.* Herpes simplex virus infection of dendritic cells: balance among activation, inhibition, and immunity. *J. Infect. Dis.* **187,** 165–78 (2003).

96. Koelle, D. M. & Corey, L. Recent progress in Herpes Simplex Virus immunobiology and vaccine research. *Clin. Microbiol. Rev.* **16,** 96–113 (2003).

97. Lu, W.-W., Sun, J.-R., Wu, S.-S., Lin, W.-H. & Kung, S.-H. A dual reporter cell assay for identifying serotype and drug susceptibility of herpes simplex virus. *Anal. Biochem.* **415,** 97–104 (2011).

98. Shapiro, H. M. *Practical Flow Cytometry*. (John Wiley & Songs, Inc., 2003).

99. Sandhu, K. S., Naciri, M. & Al-Rubeai, M. Prediction of recombinant protein production in an insect cell-baculovirus system using a flow cytometric technique. *J. Immunol. Methods* **325,** 104–13 (2007).

100. Deparis, V., Jestin, a, Marc, a & Goergen, J. L. Use of flow cytometry to monitor infection and recombinant human alpha-1,3/4 fucosyltransferase production in baculovirus infected Sf9 cell cultures. *Biotechnol. Prog.* **19,** 624–30 (2003).

101. Da Costa, X. J., Bourne, N., Stanberry, L. R. & Knipe, D. M. Construction and characterization of a replication-defective herpes simplex virus 2 ICP8 mutant strain and its use in immunization studies in a guinea pig model of genital disease. *Virology* **232,** 1–12 (1997).

102. Mundle, S. T. *et al.* High-purity preparation of HSV-2 vaccine candidate ACAM529 is immunogenic and efficacious in vivo. *PLoS One* **8,** e57224 (2013).

103. Delagrave, S. *et al.* Immunogenicity and efficacy of intramuscular replication-defective and subunit vaccines against herpes simplex virus type 2 in the mouse genital model. *PLoS One* **7,** e46714 (2012).

104. Tartaglia, J., Gurunathan, S., Kim, J. H. & Francis, D. Immunological Compositions for HIV. (2012).

105. Armbruster, D. a & Pry, T. Limit of blank, limit of detection and limit of quantitation. *Clin. Biochem. Rev.* **29 Suppl 1,** S49–52 (2008).

106. Shrivastava, A. & Gupta, V. Methods for the determination of limit of detection and limit of quantitation of the analytical methods. *Chronicles Young Sci.* **2,** 21 (2011).

107. Wymer, J. P., Chung, T. D., Chang, Y., Hayward, G. S. & Aurelian-, L. Identification of Immediate-Early-Type cis-Response Elements in the Promoter for the Ribonucleotide Reductase Large Subunit from Herpes Simplex Virus Type 2. **63,** 2773–2784 (1989).

108. Zhu, J. & Aurelian, L. AP-1 cis-response elements are involved in basal expression and Vmw110 transactivation of the large subunit of herpes simplex virus type 2 ribonucleotide reductase (ICP10). *Virology* **231,** 301–312 (1997).

Appendix A

Cell Age Study

It was found that the passage number of the cells had a significant effect on the total number of HSV2013-121 cells which demonstrated an elevated level of granularity. It was previously known that cell growth slowed after approximately 20 passages, but nothing else was known of consequence of the cells after n+20. Here, it is demonstrated that as the age of the cell increases, the maximum number of cells displaying high granularity diminishes.

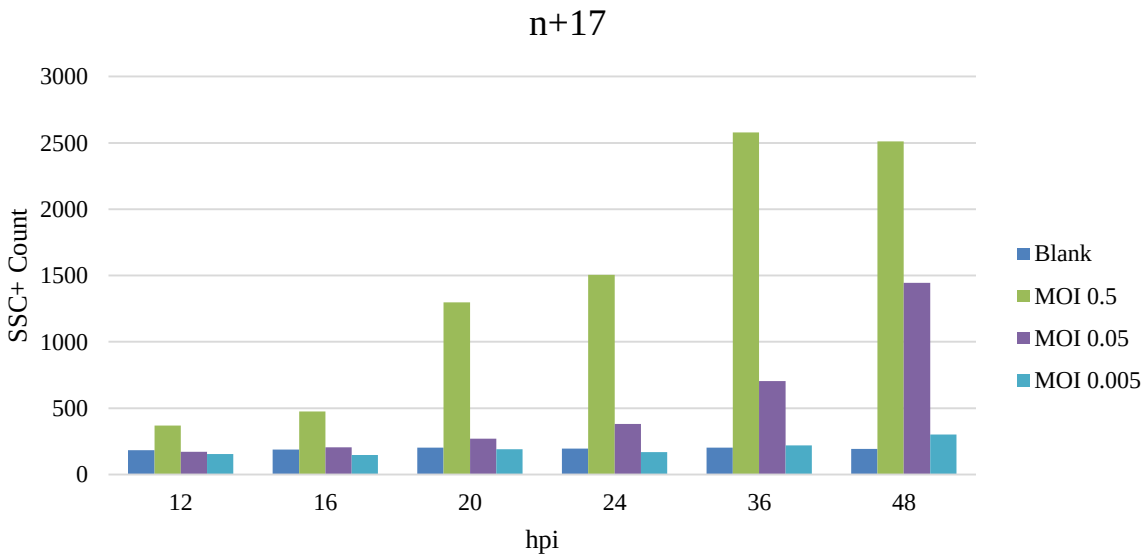

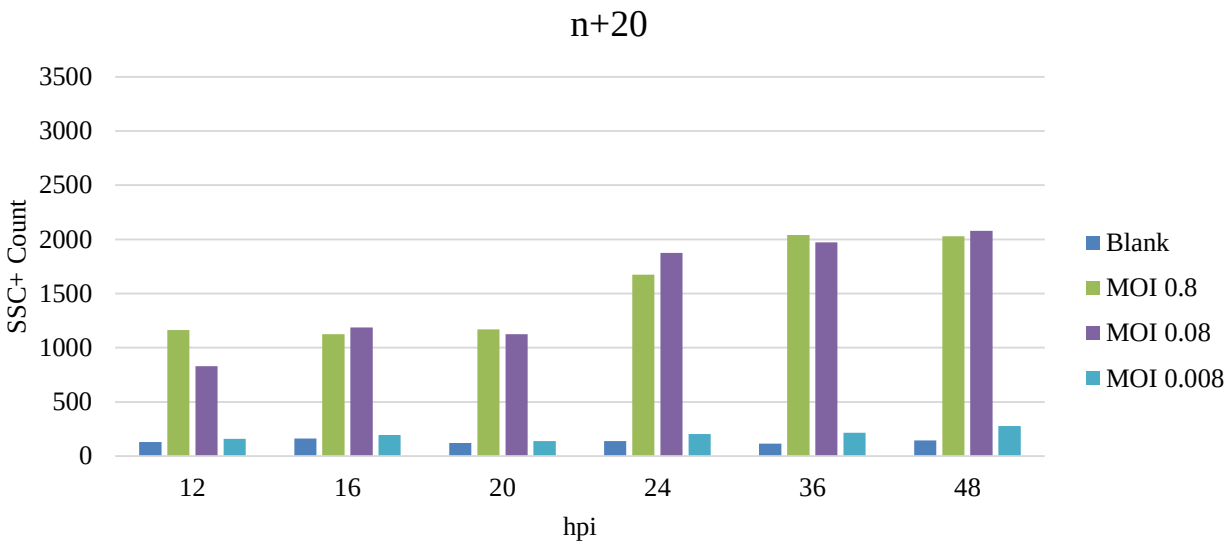
n+20
3500
3000
2500
2000
1500
1000
500
0
SSC+ Count
12
16
20
24
36
48
hpi
Blank
MOI 0.8
MOI 0.08
MOI 0.008

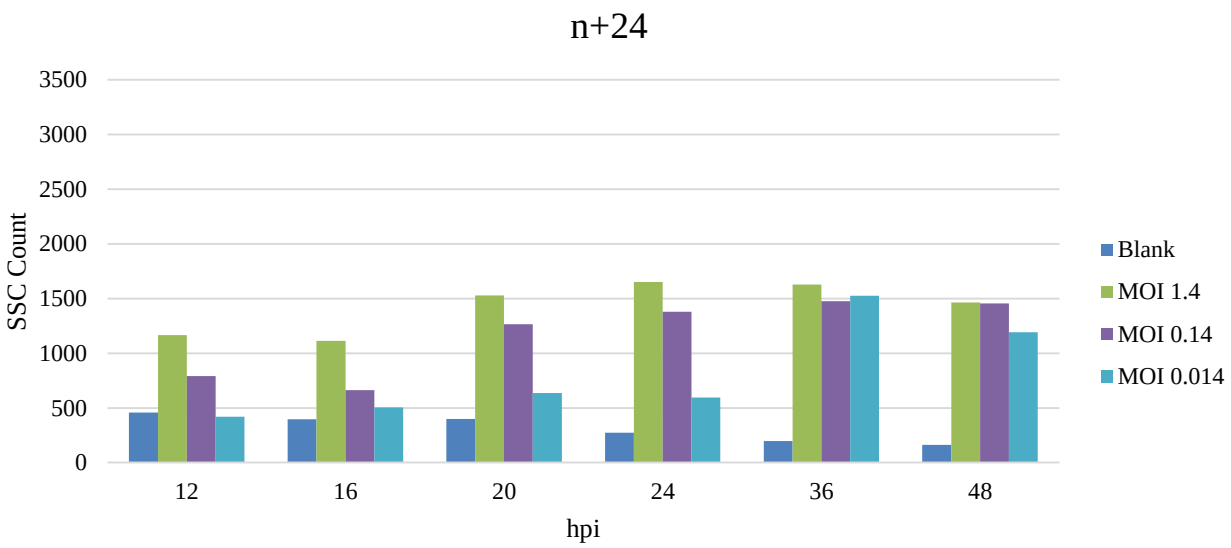
n+24
3500
3000
2500
2000
1500
1000
500
0
SSC Count
12
16
20
24
36
48
hpi
Blank
MOI 1.4
MOI 0.14
MOI 0.014